NAVAL POSTGRADUATE SCHOOL

MONTEREY, CALIFORNIA

THESIS

DIVER-APPLIED UNDERWATER COMPOSITE PATCH REPAIR ON ALUMINUM HULLS

by

Robyn W. Bianchi

September 2018

Thesis Advisor:	Young W. Kwon
Co-Advisor:	Erick S. Alley
Second Reader:	Jarema M. Didoszak

THIS PAGE INTENTIONALLY LEFT BLANK

REPORT DOCUMENTATION PAGE			*Form Approved OMB No. 0704-0188*

1. AGENCY USE ONLY *(Leave blank)*	**2. REPORT DATE** September 2018	**3. REPORT TYPE AND DATES COVERED** Master's thesis

4. TITLE AND SUBTITLE DIVER-APPLIED UNDERWATER COMPOSITE PATCH REPAIR ON ALUMINUM HULLS	**5. FUNDING NUMBERS**
6. AUTHOR(S) Robyn W. Bianchi	
7. PERFORMING ORGANIZATION NAME(S) AND ADDRESS(ES) Naval Postgraduate School Monterey, CA 93943-5000	**8. PERFORMING ORGANIZATION REPORT NUMBER**
9. SPONSORING / MONITORING AGENCY NAME(S) AND ADDRESS(ES) N/A	**10. SPONSORING / MONITORING AGENCY REPORT NUMBER**

11. SUPPLEMENTARY NOTES The views expressed in this thesis are those of the author and do not reflect the official policy or position of the Department of Defense or the U.S. Government.

12a. DISTRIBUTION / AVAILABILITY STATEMENT Approved for public release. Distribution is unlimited.	**12b. DISTRIBUTION CODE** A

13. ABSTRACT (maximum 200 words)

This thesis investigates the feasibility of applying a composite repair patch in the underwater environment as an alternative repair on aluminum ship hulls over conventional welding and replacement repairs, which can be too costly and time consuming. An aluminum sample with a machined hole was chosen as the defected material to repair. After much research and leveraging of NSWCCD's approved topside composite repair procedure, a composite repair patch with E glass and a chosen underwater epoxy was selected. In a controlled laboratory setting, in two experiments, 24 different patched samples were tested for tensile load and a bending moment. Strain, load, and displacement were measured and compared with the baseline composite patch performance characteristics. A model was developed for each test using finite element analysis to predict the different stress data, and was used to investigate failure modes. The primary property used as a comparison for patch performance was strain, which was measured using strain gauges and numerically derived using FEA. The results showed that, in both loading conditions, the underwater composite repair patches were successful at significantly decreasing the strain at the hole (i.e., the location of maximum strain concentration). Both experiments also showed that the interface strength increased as the underwater cure time of the patch increased.

14. SUBJECT TERMS composite repair, underwater repair, Navy Ship repair	**15. NUMBER OF PAGES** 113
	16. PRICE CODE

17. SECURITY CLASSIFICATION OF REPORT	**18. SECURITY CLASSIFICATION OF THIS PAGE**	**19. SECURITY CLASSIFICATION OF ABSTRACT**	**20. LIMITATION OF ABSTRACT**
Unclassified	Unclassified	Unclassified	UU

NSN 7540-01-280-5500 Standard Form 298 (Rev. 2-89) Prescribed by ANSI Std. 239-18

THIS PAGE INTENTIONALLY LEFT BLANK

Approved for public release. Distribution is unlimited.

DIVER-APPLIED UNDERWATER COMPOSITE PATCH REPAIR ON ALUMINUM HULLS

Robyn W. Bianchi
Lieutenant, United States Navy
BS, U.S. Naval Academy, 2011

Submitted in partial fulfillment of the
requirements for the degree of

MASTER OF SCIENCE IN MECHANICAL ENGINEERING

from the

NAVAL POSTGRADUATE SCHOOL
September 2018

Approved by: Young W. Kwon
Advisor

Erick S. Alley
Co-Advisor

Jarema M. Didoszak
Second Reader

Garth V. Hobson
Chair, Department of Mechanical and Aerospace Engineering

THIS PAGE INTENTIONALLY LEFT BLANK

ABSTRACT

This thesis investigates the feasibility of applying a composite repair patch in the underwater environment as an alternative repair on aluminum ship hulls over conventional welding and replacement repairs, which can be too costly and time consuming. An aluminum sample with a machined hole was chosen as the defected material to repair. After much research and leveraging of NSWCCD's approved topside composite repair procedure, a composite repair patch with E glass and a chosen underwater epoxy was selected. In a controlled laboratory setting, in two experiments, 24 different patched samples were tested for tensile load and a bending moment. Strain, load, and displacement were measured and compared with the baseline composite patch performance characteristics. A model was developed for each test using finite element analysis to predict the different stress data, and was used to investigate failure modes. The primary property used as a comparison for patch performance was strain, which was measured using strain gauges and numerically derived using FEA. The results showed that, in both loading conditions, the underwater composite repair patches were successful at significantly decreasing the strain at the hole (i.e., the location of maximum strain concentration). Both experiments also showed that the interface strength increased as the underwater cure time of the patch increased.

THIS PAGE INTENTIONALLY LEFT BLANK

TABLE OF CONTENTS

LIST OF FIGURES

LIST OF TABLES

THIS PAGE INTENTIONALLY LEFT BLANK

LIST OF ACRONYMS AND ABBREVIATIONS

Al	Aluminum
EPF	Expeditionary Fast Transport Ship
FEA	Finite Element Analysis
FRP	Fiber Reinforced Polymers
LCS	Littoral Combat Ship
NA	Neutral Axis
NAVSEA	Naval Sea Systems Command
NSTM	Navy Ships Technical Manual
NSWCCD	Naval Surface Warfare Center Carderock Division

THIS PAGE INTENTIONALLY LEFT BLANK

ACKNOWLEDGMENTS

I would like to take the opportunity to extend my deepest gratitude for all who helped me in the successful completion of my thesis. First, I would like to thank my thesis advisor, Professor Young Kwon, for his endless dedication, patience, and guidance throughout the thesis process. The material you introduced engaged my interest in the field of solid mechanics and allowed true innovation with my thesis work. Thank you for your advice and counsel while I conducted my research and explored the uncharted work of working with composites in the underwater environment. I would also like to thank Dr. Erick Alley, Professor Jarema Didoszak, Mr. John Mobley, Mr. Levi Owen, and Dr. Chanman Parks for their support and guidance during the testing phase of my thesis.

Finally, I would like to thank my husband, Dr. Christopher Bianchi, for his unwavering support of my graduate studies and teaching me that science and mathematics is the most beautiful language in the universe. Thank you for reminding me continuously not to worry about grades, but, instead, to focus on understanding the dialects of this beautiful language and to maintain a curious mind, and to continue feeding my desire for more.

THIS PAGE INTENTIONALLY LEFT BLANK

I. INTRODUCTION AND BACKGROUND

A. U.S. NAVY COMPOSITE REPAIR (DRY ENVIRONMENT)

Composite repair patching is currently providing an alternative solution over other conventional repairs to U.S. Navy ships that are susceptible to stress corrosion cracking and fatigue cracking. Specifically, the superstructure of the Ticonderoga-class cruisers, which is composed of aluminum alloy 5456, has been determined to be susceptible to cracking in the aluminum alloy [1]. The Navy recognized that this aluminum alloy will become sensitized at higher temperatures as a result of the incorrect heat treatment processing received during the manufacturing process. As a result of this sensitization, there have been many issues with cracking in the aluminum [1], [2]. Sensitization refers to a harmful microstructure that increases the corrosion susceptibility in Al 5XXX series alloys. Sensitized Al is observed in 5XXX alloys that have magnesium contents greater than 3 percent weight content and operate at temperatures reached by simple solar exposure [1].

A composite material is defined as "a combination of two or more different materials on a macroscopic scale, with different physical and/or chemical properties, which form a useful third material resulting in different characteristics (often stronger) than the original materials" [2].

Conventional repairs necessary in this "dry environment" include completely cutting out and removing the affected sections, and conducting hot work (welding) repairs. In some situations a weld repair cannot be performed, as called out in ASTM G67, which states a mass loss greater than 60 mg/cm^2 cannot be welded because cracks will form in the area adjacent to the weld repair [3].

These conventional repairs are time consuming and costly. A comparison of aluminum repair costs between composite repairs and weld repairs shows that the composite patch repairs are significantly lower than the weld repairs made [4].

The U.S. Navy began to consider the successful Royal Navy repair procedures using composite patching for the Type 21 frigates in 1983. These frigates experienced

fatigue cracks in the aluminum alloy superstructures, much like the U.S. Navy Ticonderoga-class cruisers. The Royal Navy attempted to conduct conventional weld repairs on these cracks, but these repairs proved to be ineffective and failed within a short time period after the repair was conducted [5]. The use of a carbon fiber reinforced epoxy patch was employed as an alternative repair application. After a successful trial use of this composite patching, the Royal Navy began to use this type of repair on seven of its ships [5]. These ships are still in service to date, having been sold to Pakistan in 1993. At the time of the sale, all the repairs made using composite patching procedure were still operating effectively with no cracking found beneath any of the patch sites. The Royal Navy and its Type 21 Frigates case study have shown the U.S. Navy that a composite repair patch procedure is an effective alternative to conventional repairs. It has also shown that this type of repair could be considered durable, and potentially classified as a long-term temporary repair lasting at least 10 years in service [5].

After much research and experimentation with alternative repair methods in hopes of avoiding the conventional repairs of welding or complete replacement of affected areas, the U.S. Navy has developed an approved procedure to repair the affected aluminum alloy area of concern and prevent crack growth while restoring the integrity of the compromised area utilizing composite patching [6]. This repair patch and procedure was developed by Naval Surface Warfare Center Carderock Division (NSWCCD) and serves as a temporary solution for the topside repair. The procedure currently does not recover the absolute structural integrity of the affected area, but is used as a long-term repair. The U.S. Navy has applied this alternative composite repair patch procedure to the 5456-H116 aluminum alloy superstructures and deck aboard CG-47 class ships, and is currently in service aboard eleven different ships of that class [6].

NSWCCD technical report [6] includes the complete process and procedure for the approved composite patch repair. In this report, the composite patch development, materials, procedures, and application procedure are described in full detail.

B. COMMERCIAL COMPOSITE REPAIR (WET ENVIRONMENT)

The underwater environment is harsh and unforgiving, especially to man-made systems. Offshore structures are subjected to severe environmental and operational conditions. These conditions, which consist of exposure to corrosion, external impacts and exposure to operational stresses and fatigue loads, can cause minor and major damage to these structures. As a result, repairs are relatively frequent and depending on the system, can range from underwater welding to utilizing coffer dams for dry repairs. These repairs have proven to be costly and time consuming, and in some instances have proven ineffective. Many different commercial activities have begun to explore the use of a water-activated resin and fiber reinforced polymers (FRP) of carbon or glass to conduct emergency repairs.

There are many successful examples of repairing corrosion-damaged, stress fatigue damage, and impact damaged systems in the underwater environment. In the Southeastern United States, the University of South Florida is conducting ongoing research and experiments to evaluate the feasibility of using FRP for repairing corrosion-damaged concrete piles of an old bridge [7]. The Gandy Bridge that spans Tampa Bay has seventy seven percent of the 254 piles that have needed to be repaired due to the corrosion environment [7]. The study conducted at the University of South Florida consisted of selecting piles to repair using an underwater FRP repair procedure. Two application methods, a pre-preg “pre-impregnated with a particular resin” system developed by Air Logistics [8], and a wet-layup system developed by FYFE [9] were studied; both methods used carbon and glass. Both used a water-activated underwater epoxy. The conclusion of the Gandy Bridge study showed that the consideration and feasibility of using a composite patch as an alternative to conventional bridge repairs could be extremely cost-effective and should be considered [7].

Another commercial example of using a composite repair procedure in the underwater environment is Subsea Pipeline repair. In a report prepared for presentation at the Abu Dhabi International Petroleum Exhibition & Conference held in Abu Dhabi in November 2012, composite repair solutions for restoring structural integrity of damaged pipelines were discussed [10]. The report describes how a composite repair system can

provide hoop stress and axial stress resistance, allowing the damaged pipeline to be repaired to resist tension and bending forces as well as internal pressure forces [10]. The tests performed in the study established that it is possible to adapt a composite repair system for subsea use and concluded this possibility has many advantages over conventional methods of repair [10].

C. BENEFIT OF STUDY

Aluminum has become a common structural material in different classes of U.S. Naval vessels due to its weight advantage over other structural materials, such as steel. Specifically, the Independence class Littoral Combat Ships (LCS) and the Expeditionary Fast Transport (EPF) ships have utilized aluminum for structural components in the hulls and superstructures. As stated earlier, the benefits of using aluminum come with its own challenges that can affect the structure's life cycle, such as stress corrosion cracking, fatigue and sensitization.

NSTM 100 requires ship structures that have experienced a reduced thickness due to corrosion to be repaired via welding or replacement [11]. Repair by replacement or welding is a current repair strategy that has proved problematic due to the loss of strength observed near the welded areas, and frequent repairs have been needed. The base concept of using a composite repair procedure to conduct these repairs instead of welding and replacement has been proposed and developed to arrest the cracks and damage for a topside application.

Supervisor of Salvage and Diving (NAVSEA OOC), along with its diving services contractor, has developed an underwater hyperbaric aluminum welding capability to address potential hull cracks on the Independence class LCS and the EPF class underwater hulls. The use of cofferdams or hyperbaric environments could prove to be too costly and time consuming; depending on operational status of the vessel, it may not even be feasible. An example of damages to the underwater hulls is shown in Figure 1 and Figure 2.

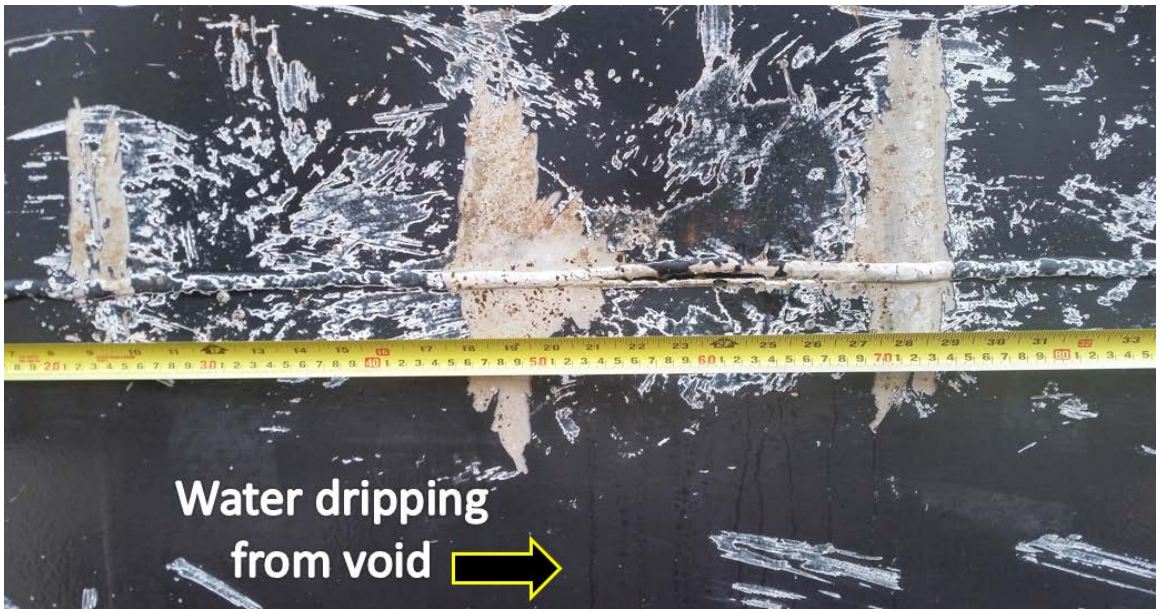

Figure 1. USS *Coronado* (LCS-4) Underwater Cracks along Weld Seam. Source: [4].

Figure 2. USS *Coronado* Underwater Cracks: Vertical and Horizontal along Weld Seam. Source: [4].

Unlike previous studies discussed with the application of composite repair patching above and below the waterline, this study is primarily concentrated with the feasibility of applying a composite repair patch directly to the damage in the underwater environment as a potentially faster and less costly repair. As previously stated, the current method for repair above the waterline is placing a composite patch over the crack in order to redistribute the stress that occurs around the crack and to the composite. There currently is no composite patch method for repair of a hull crack in the underwater environment. The application of a composite patch directly underwater is focused on providing Navy divers the ability to execute a composite patch externally to the hull as a temporary repair to allow the ship to continue on its mission or return to port for more permanent repairs. This study has the following goals:

1. Confirm that the patch can be installed in the underwater environment to potential aluminum hull cracks utilizing a wet lay-up method described in reference [6] with required adhesion and structural strength.

2. Determine what maximum static loading condition this specific composite patch could withstand.

3. Measure the maximum bending loading this specific composite patch could withstand.

This study will explore an alternative repair possibility for the Navy and Department of Defense to conduct emergent underwater repairs utilizing composite repair patching techniques that could be accomplished by Navy divers.

II. EXPERIMENTAL PROCEDURE

A. SAMPLE SPECIFICATION

1. Aluminum Sample

The overall goal of this study is to determine whether a composite repair patch can be employed in the underwater environment to an aluminum hull of a damaged ship. From the introduction, it is shown that no testing or study that has been conducted for this application. There are many different variables that could be experienced in the underwater environment along with many different types of damages that a ship's hull could experience and that a composite patch could be used for. To provide a baseline of data for comparison and results, this study is limited to a single sample selection in which multiple tests will be conducted.

The sample material chosen that is used to model the hull of a ship is a 5052 H32 aluminum alloy. The defect size and shape chosen that is used to model the defect in the hull of a ship is in the form of a machined hole. It was decided to use a machined hole over a crack due to the limitations of the machine shop's ability to create a consistent defect throughout all samples and to ensure all data collected from each test could be comparable to each other. The dimensions of the test specimens and defect used throughout this study are shown in Figure 3 with the corresponding dimensions and material properties in Table 1.

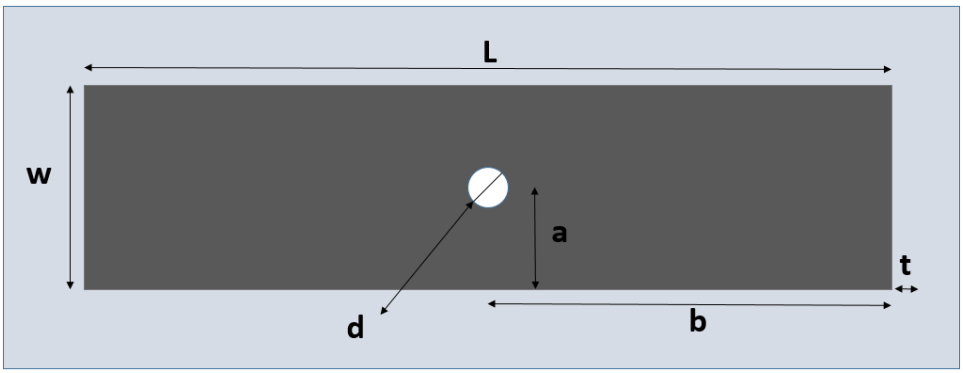

Figure 3. Aluminum Sample Design with Machined Hole

Table 1. Aluminum Sample Dimensions and Material Properties

Sample Dimensions	
Thickness (t)	0.002032 m
Width (w)	0.1016 m
Length (L)	0.3048 m
Diameter (d)	0.0127 m
Hole Vertical Offset (a)	0.508 m
Hole Horizontal Offset (b)	0.1524 m
Moment of Inertia (Izz)	7.1037e-11 m^4
Material Properties Al 5052 H-32	
Ultimate Tensile Strength	228 MPa
Ultimate Yield Strength	180 MPa
Modulus of Elasticity	74.3 Gpa
Density	2679.436 kg/m^3

2. Composite Patch Sample

a. Materials

(1) Resin and Hardener

For this study Tyfo SW-1 Epoxy, made by FYFE Co. LLC, was used for the resin and hardener. “This two part, 100% solids epoxy formulation consists of epoxy resins, hardeners and inert fillers, and is specifically designed for underwater applications” [12]. As mentioned in the introduction, this specific underwater epoxy was used in the repairs to the Granby Bridge in Southern Florida and was chosen for this study for its successful use in the wet lay-up method of the Gandy Bridge study. The Tyfo SW-1 Epoxy is a two part preparation consisting of Part A (base) and Part B (hardener) [12]. The material properties of the Epoxy itself are shown in Figure 4. The SW-1 Epoxy is used in the underwater environment and should be mixed above water and then transported below water to the depth of repair. Part A and Part B are premixed individually and then should be combined in a clean container and mixed together thoroughly [12]. The mixing ratio is “100 parts of component A to 74 parts of component B by volume. (100 parts of component A to 56

parts of component B by weight)" [12]. The SW-1 Epoxy should be applied in water temperatures above 277.6 K.

Typical Material Properties at 75° F.	
Mixing ratio, by wt.	100:56
Specific Gravity	1.6
Viscosity A & B mixed, cps	14,000 - 18,000
Gel Time, 65° F, hours	2.5 - 3.5
ASTM D695, 7 day compressive strength, psi	7,000 - 8,000
ASTM D695, 7 day compressive strength, mortar, psi (gel/uw:sand – 1:1 by volume)	8,000 - 9,000
ASTM D2240 Shore D hardness	80 - 85

Figure 4. SW-1 Epoxy Material Properties. Source: [12].

(2) E glass

For this study, 7500 Hexcel 6 ounce plain weave E glass fabric was used for the layers during the wet-layup procedure of the patch fabrication. This specific type of E glass fabric has a thickness of 0.236 mm, and is described by the manufacture as "a lightweight cloth employed in the small craft boat building industry" [13]. Each layer of dry E glass fabric used in the laminate stack while building up the patch is considered a plie. For this study, eight plies were used in accordance with the approved procedure developed by NSWCCD for topside patching [6].

(3) Tools/Equipment

The tools and equipment utilized to create each sample include:

Aluminum Sample (pre-fabricated with hole)

E glass

SW-1 Epoxy

Vacuum Bag

Powder Free Latex Gloves

Lint Free Rags

Underwater work bench

C-clamps

Distilled Water

Sodium

Plastic tank (200-gallon, filled with a 3.5% salt solution mixed from Distilled water and sodium)

Mixing Containers

Tongue Depressors

Squeegees

Scissors

Fabric Cutting Wheel/Board with Ruler

Safety Goggles

3M Surface Preparation Metal Cleaner

b. Lamination Procedures

(1) Dry Patching

The lamination process for the dry patching follows NSWCCD approved procedure as closely as possible to ensure the highest quality laminate is achieved with the exception

of using a vacuum source while patch cures. The process consists of measuring and cutting dry fabric for the laminate stack, mixing the resin, and conducting the wet-out of the fabric directly onto location of hole, allowing the patch to air cure.

The following procedure describes the process of conducting a single dry patch, using the SW-1 Epoxy and E glass above the water and allowing to air cure. The full process is photographed for reference in Appendix A.

1. Measure and cut the E glass so that four plies have a 90 degree fiber orientation and four plies have a 45 degree fiber orientation and all are approximately .1524m (6in) in length and .1016m (4in) in width.

2. Place Aluminum Sample with hole onto a sturdy surface.

3. Mix Part A (base) and Part B (hardener) individually at 100:74 by volume or 100:56 by weight. [12] Combine together in a clean container and mix thoroughly until well combined.

4. Use tongue depressor to wet out repair area surface (6in x 4in) with epoxy mixture and apply the first ply directly onto wet out area. Using squeegees, impregnate ply and remove as much air as possible, ensuring entire ply is wet-out.

5. Repeat step 5 for the remaining 7 plies. Ensure that the ply stack orientations are correct in regard to fiber direction. Ply schedule is [(0/90)/(-45/45)/(0/90)/(-45/45)/(0/90)/(45/-45)/(90/0)/(45/-45)].

6. Allow to fully cure: minimum 24 hours recommended

(2) Wet Patching

The lamination process for the wet patching follows NSWCCD approved topside procedure as closely as possible, but due to the underwater environment, this study explores innovative ways to conduct the patching underwater. The process described is the method used for this study, but is recommended that further refinement and efficiency be

researched in the future for real-world application for the many different environments that would be experienced.

The process consists of measuring and cutting dry fabric for the laminate stack, mixing the resin, and conducting the wet-out of the fabric directly onto the vacuum bag sheet, ensuring the stack is in line one on top of the other. Once the wet-build up is completed, the patch shall be handled by the vacuum bag sheet and brought into the tank full of water and placed onto the sample. Prior to beginning the patching procedure, the sample shall be pre-staged onto the underwater work bench and held static via two C-clamps.

The following procedure describes the process of conducting a single wet patch, using the SW-1 Epoxy and E glass in a 3.5% salt solution underwater environment and allowing to cure for at a minimum of 24 hours. The full process is photographed for reference in Appendix A.

1. Measure and cut the E glass so that four plies have a 90 degree fiber orientation and four plies have a 45 degree fiber orientation and all are approximately .1524m (6in) in length and .1016m (4in) in width.

2. Stage Aluminum Sample with hole onto the underwater work bench in the 200 gallon tank full of 125 gallons of 3.5% salt solution distilled water. Clamp sample to ensure it is static.

3. Mix Part A (base) and Part B (hardener) individually at 100:74 by volume or 100:56 by weight [12]. Combine together in a clean container and mix thoroughly until well combined.

4. Using tongue depressor, wet out vacuum bag sheet area surface (6in x 4in) with epoxy mixture and apply the first ply directly onto epoxy. Using squeegees, impregnate ply and remove as much air as possible, ensuring entire ply is wet-out.

5. Repeat step 5 for the remaining 7 plies. Ensure that the ply stack orientations are correct in regards to fiber direction. Ply schedule is [(0/90)/(-45/45)/(0/90)/(-45/45)/(0/90)/(45/-45)/(90/0)/(45/-45)].

6. Take hold of the patch by grabbing the bottom of the vacuum bag material so that the patch is being held on hands under the vacuum bag material.

7. Submerge patch carefully and flip the vacuum bag material over such that the wet epoxy patch is directly over the aluminum sample.

8. Align the patch over the hole and press down gently to place patch.

9. Firmly apply pressure and adjust patch to ensure it is correctly aligned onto sample.

10. Keep the vacuum bag sheet on top of the sample until cure time is complete.

11. Allow to fully cure: minimum 24 hours recommended

3. Concept of Experimental Testing

A ship's hull experiences many different complex and combined loads and strains during at sea operations. The technical objective of this study is to demonstrate the performance of the underwater composite repair system on a sample level. The study will focus on two basic types of loading conditions. The first being a four point bending test which will simulate basic loading conditions a ship's hull will experience while at sea and analyze how the patch will respond. The second being a tensile pull test which will analyze interface strength and load carrying characteristics of the patch.

a. Experiment I: Four Point Bending Test

Experiment I of this study consists of performing a quasi-static four point bending test on many different samples while recording the load, displacement, and strain. The four point bending test is representative of basic loading conditions at a sample level of an

underwater hull panel bending during at sea operations. The technical objective of this test is to demonstrate how effective the application of an underwater composite repair patch is at decreasing the strain at the defect when compared to a sample without a patch. The four-point bending test consists of the sample specimen being placed on two bottom roller supports and a load is applied by two top rollers. These top rollers are mounted symmetrically in the middle of the loading span to ensure a uniformly distributed bending moment is experienced on the center section of the sample, with a normal tensile stress developed in the convex (bottom) side of the sample, and a normal compressive stress is generated on the concave (top) side of the sample. The top and bottom testing devices are shown in Figure 5 and are in accordance with ASTM standard G39-99 [14].

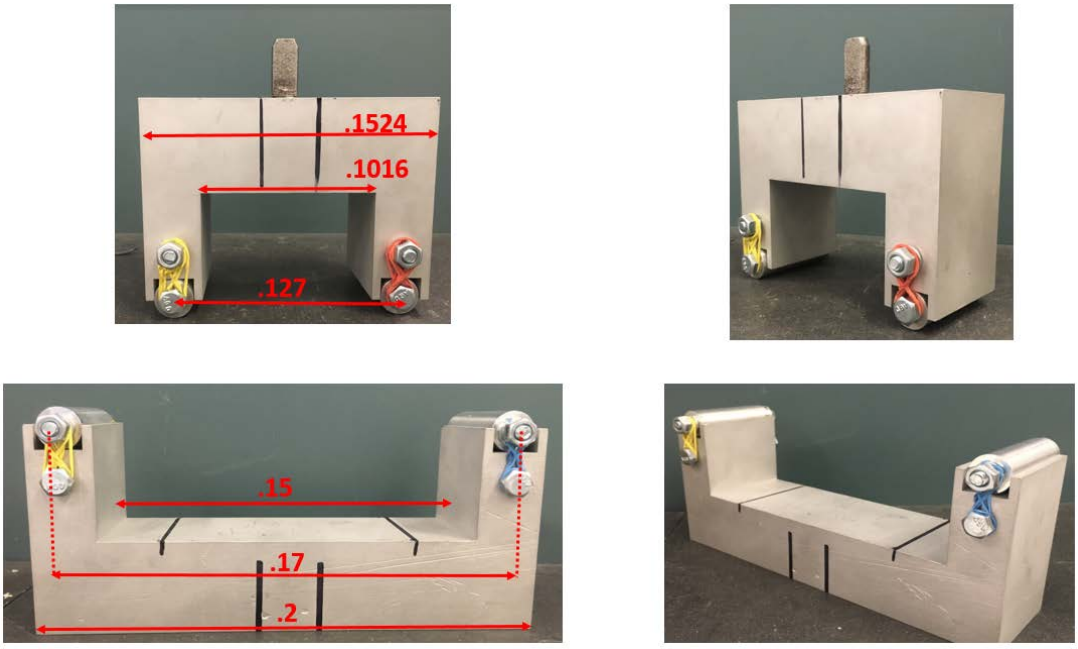

Figure 5. Four Point Bending Device: Top and Bottom
(dimensions in meters)

b. Experiment II: Static Tensile Pull Test

Experiment II of this study consists of performing a quasi-static tensile pull test on many different samples while recording the load, displacement, and strain. The tensile pull test will demonstrate the application of the bonded composite repair patch and analyze the interface strength of the composite to the aluminum sample as well as capture the load carrying characteristics of the patch.

4. Testing Matrix

This study conducted two separate experiments modeling basic loading conditions and consisted of testing six different samples. The six different samples tested for each experiment are described in the following:

1. Two samples with machined hole and no patch. Baseline Testing.

2. Two samples with machined hole and a composite repair patch conducted above the water and allowed to cure in the dry environment.

3. Two samples with machined hole and a composite repair patch conducted above the water, applied to a submerged sample, and allowed to cure in the 3.5% NaCl water solution for 24 hours.

4. Two samples with machined hole and a composite repair patch conducted above the water, applied to a submerged sample, and allowed to cure in the 3.5% NaCl water solution for 1 week.

5. Two samples with machined hole and a composite repair patch conducted above the water, applied to a submerged sample, and allowed to cure in the 3.5% NaCl water solution for 2 weeks.

6. Two samples with machined hole and a composite repair patch conducted above the water, applied to a submerged sample, and allowed to cure in the 3.5% NaCl water solution for 4 weeks.

The samples throughout the study will be referenced based on the testing matrix shown in Table 2.

Table 2. Testing Matrix for Experiments I and II

Experiment I: Four-Point Bending Load				
Sample	No Patch	Patch		
		Dry	Wet	Time in Water
A	X			
B	X			
C		X		
D		X		
E			X	24 HOURS
F			X	24 HOURS
G			X	1 WEEK
H			X	1 WEEK
I			X	2 WEEKS
J			X	2 WEEKS
K			X	4 WEEKS
L			X	4 WEEKS

Experiment II: Static Tensile Load				
Sample	No Patch	Patch		
		Dry	Wet	Time in Water
A	X			
B	X			
C		X		
D		X		
E			X	24 HOURS
F			X	24 HOURS
G			X	1 WEEK
H			X	1 WEEK
I			X	2 WEEKS
J			X	2 WEEKS
K			X	4 WEEKS
L			X	4 WEEKS

B. EXPERIMENT I: FOUR-POINT BENDING TEST

For the four-point bending test, the MTS 858 was used as the primary testing equipment. The MTS 858 table top system using the TestStarIIs program has a maximum loading of 10 kN [15]. This is above the maximum load to ensure the region around the hole and between the rollers would transition into the plastic region. For each sample in the test matrix for Experiment I shown in Table 2, four uniaxial strain gauges were applied to measure the longitudinal strain at various locations of the samples as shown in Appendix B. The placement of these strain gauges was chosen to ensure the region around the hole would be properly captured as load increases during the testing. The uniaxial strain gauges were Omega part number SGD-7/350-LY11. The MTS procedure was set to start at 0 kN and load at a rate of 100 N/min until 935 N was reached in which case the test continued until delamination occurred. The bottom and top four point bending devices were aligned in the MTS grips to ensure symmetry while loading. For each test, the sample was placed

upon the bottom device and the top device was lowered until there was 10 N of load. Before each test, the load and displacement was set to zero.

The thickness of the patches for each sample tested in Experiment I are shown in Table 3. The MTS testing apparatus was not consistent with the maximum loads for each test. Due to this discrepancy, each sample was loaded to a different maximum load. Table 4 shows the maximum machine loads for each sample test.

Table 3. Experiment I Samples A-L Patch Thicknesses

Experiment I: Four-Point Bending Load	
Sample	Patch Thickness [m]
A	N/A
B	N/A
C	0.00366
D	0.00365
E	0.00274
F	0.00256
G	0.00322
H	0.00320
I	0.00274
J	0.00338
K	0.00323
L	0.00320

Table 4. Experiment I: Sample A-L Max Machine Loading

Experiment I: Four-Point Bending Load	
Sample	Max Machine Load [N]
A	946.47835
B	957.48274
C	2706.22829
D	2711.92963
E	1017.00000
F	991.50000
G	961.44424
H	937.50566
I	1477.73191
J	1274.91651
K	1164.00000
L	1510.38984

1. Samples A and B

The first two samples of Experiment I were the samples A and B, the samples with no patches. Figure 6 shows sample A at start prior to loading, and Figure 7 shows sample A at the end of the experiment before unloading. The maximum load applied during this test is shown in Table 4. After the removal of the load, permanent deformation is visible as shown in Figure 8.

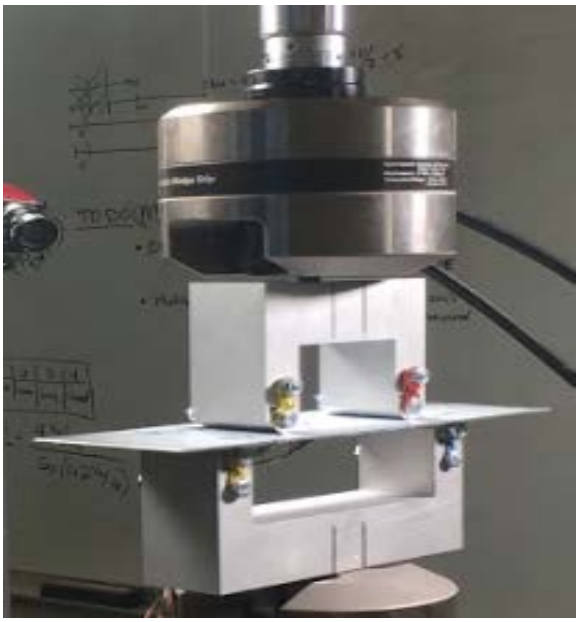

Figure 6. Experiment I: Sample A Start of Testing—Before Loading

Figure 7. Experiment I: Sample A End of Testing—Before Unloading

Figure 8. Experiment I: Permeant Deformation of Sample A

2. Samples C and D

The next pair of tests was conducted with samples C and D. These samples were patched with the dry patching procedure described earlier, but were allowed to cure above the water in a dry environment. Sample C was patched on the top side of the sample, demonstrating a dry patch in compression, and Sample D was patched on the bottom side of the sample, demonstrating a dry patch in tension. The patch thicknesses for these samples are shown in Table 3 and the maximum load applied during this test is shown in Table 4. Figure 9 show Sample C at the start of testing, prior to loading and Figure 10 show Sample C at the end of testing, before unloading. Figure 11 show Sample D at the start of testing, prior to loading and Figure 12 show Sample D at the end of testing, before unloading. After the removal of the load, permanent deformation is visible and is shown in Figure 13.

Figure 9. Experiment I: Sample C Start of Testing—Before Loading

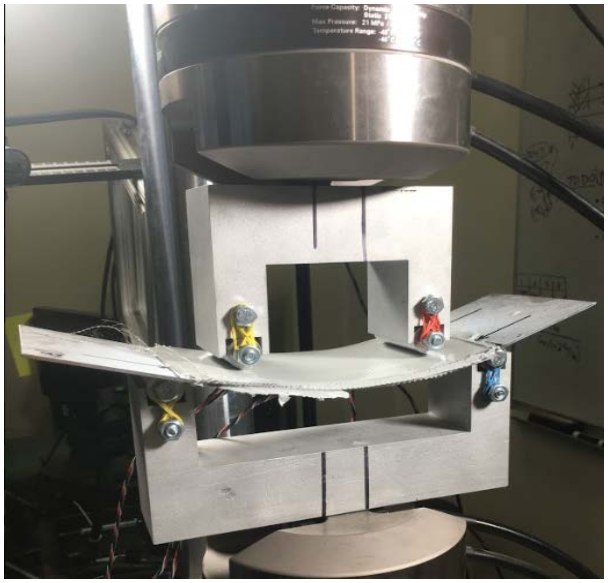

Figure 10. Experiment I: Sample C End of Testing—Before Unloading

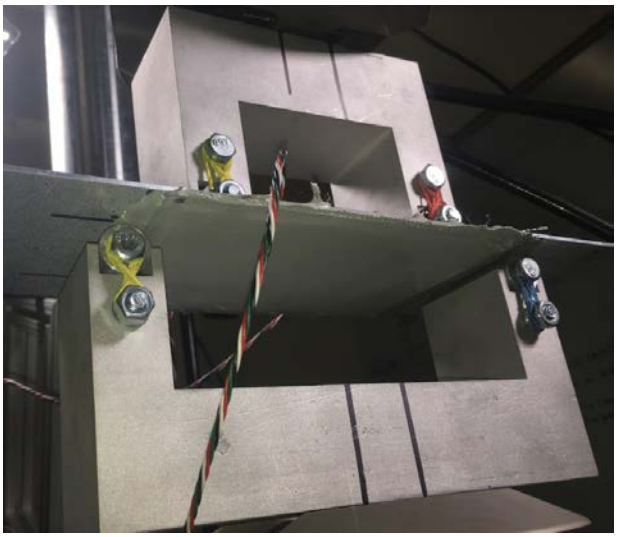

Figure 11. Experiment I: Sample D Start of Testing- Before Loading

Figure 12. Experiment I: Sample D End of Testing- Before Unloading

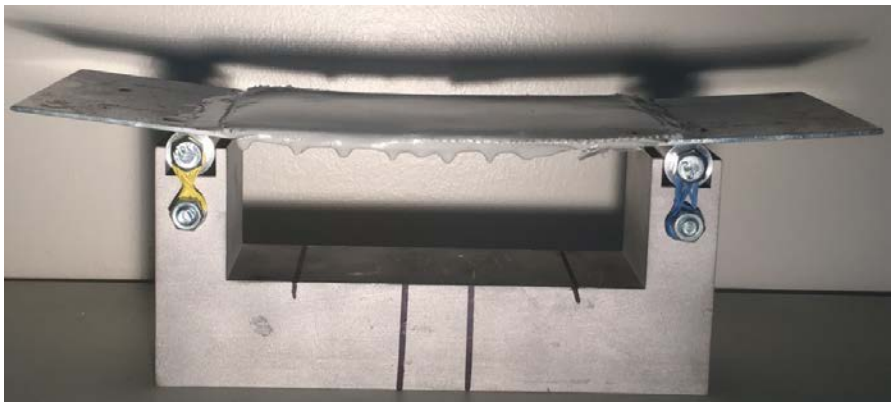

Figure 13. Experiment I: Permanent Delamination of Sample C

3. Samples E and F

The next pair of tests was conducted with samples E and F. These samples were patched with the wet patching procedure described earlier, but were allowed to cure underwater for 24 hours before being taken out and tested. Sample D and F were both patched on the top side of the sample, demonstrating a wet patch in compression. The patch thicknesses for these samples are shown in Table 3 and the maximum load applied during this test is shown in Table 4. Figure 14 show Sample E at the start of testing, prior to loading and Figure 15 show Sample E at the end of testing, before unloading. Figure 16 show Sample F at the start of testing, prior to loading and Figure 17 show Sample F at the end of testing, before unloading. After the removal of the load, there is no permanent deformation visible, this is shown in Figure 18.

Figure 14. Experiment I: Sample E Start of Testing—Before Loading

Figure 15. Experiment I: Sample E End of Testing—Before Unloading

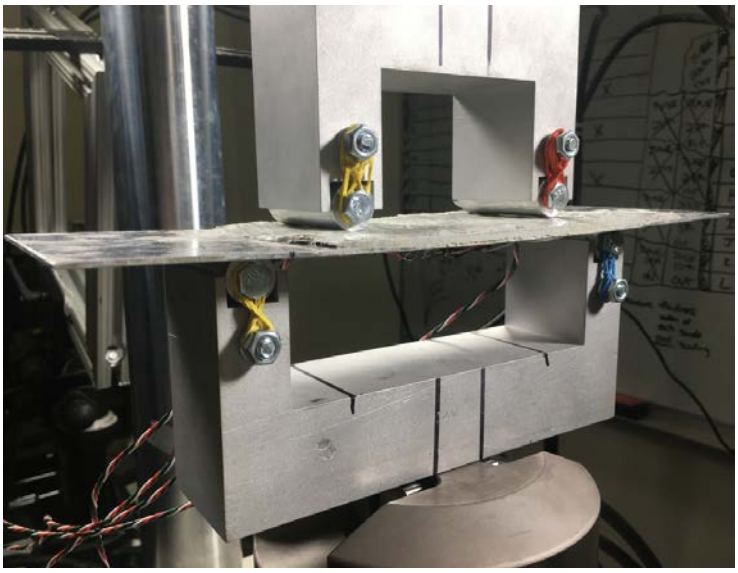

Figure 16. Experiment I: Sample F Start of Testing—Before Loading

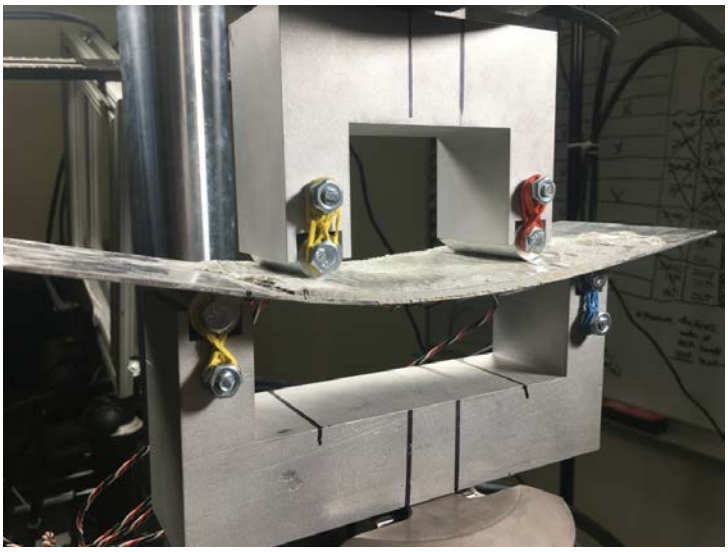

Figure 17. Experiment I: Sample F End of Testing—Before Unloading

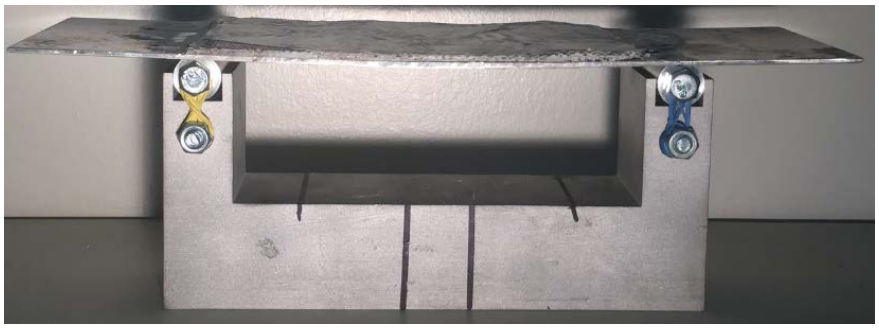

Figure 18. Experiment I: No Permanent Deformation Shown in Sample E

4. Samples G and H

The next pair of tests was conducted with samples G and H. These samples were patched with the wet patching procedure described earlier, but were allowed to cure underwater for one week before being taken out and tested. Sample G and F were both patched on the top side of the sample, demonstrating a wet patch in compression. The patch thicknesses for these samples are shown in Table 3, and the maximum load applied during this test is shown in Table 4. Figure 19 shows Sample G at the start of testing, prior to loading and Figure 20 shows Sample G at the end of testing, before unloading. Figure 21 shows Sample H at the start of testing, prior to loading, and Figure 22 shows Sample H at the end of testing, before unloading. After the removal of the load, there is no permanent deformation visible; this is shown in Figure 23.

Figure 19. Experiment I: Sample G Start of Testing—Before Loading

Figure 20. Experiment I: Sample G End of Testing—Before Unloading

Figure 21. Experiment I: Sample H Start of Testing—Before Loading

Figure 22. Experiment I: Sample H End of Testing—Before Unloading

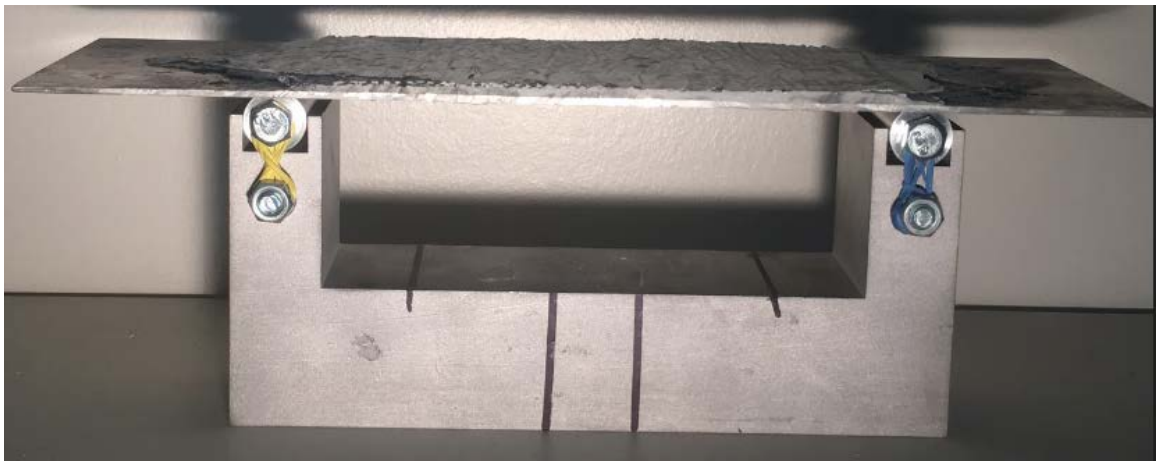

Figure 23. Experiment I: No Permanent Deformation Shown in Sample H

5. Samples I and J

The next pair of tests was conducted with samples I and J. These samples were patched with the wet patching procedure described earlier, but were allowed to cure underwater for two weeks before being taken out and tested. Sample I and J both were patched on the top side of the sample. The patch thicknesses for these samples are shown in Table 3 and the maximum load applied during this test is shown in Table 4. Figure 24 shows Sample I at the start of testing, prior to loading and Figure 25 shows Sample I at the end of testing, before unloading. Figure 26 shows Sample J at the start of testing, prior to loading and Figure 27 shows Sample J at the end of testing, before unloading. After the removal of the load, there is no permanent deformation visible; this is shown in Figure 28.

Figure 24. Experiment I: Sample I Start of Testing—Before Loading

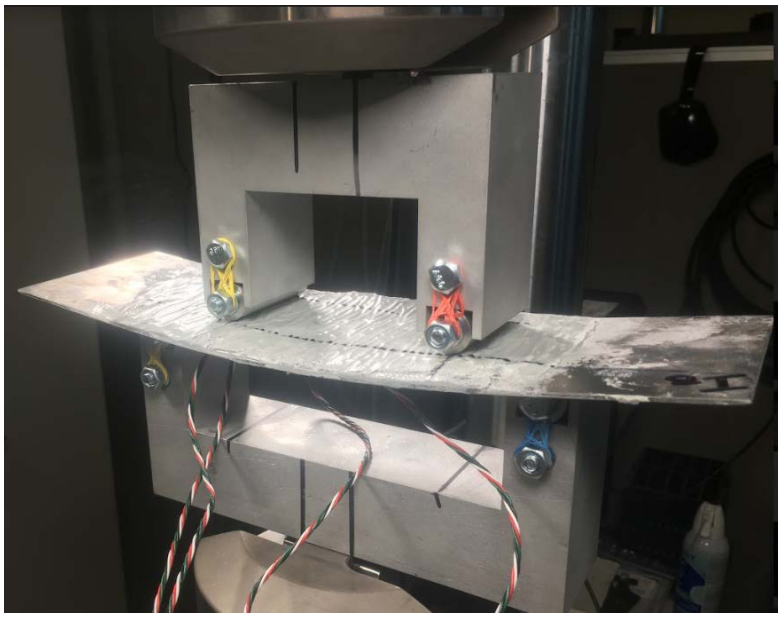

Figure 25. Experiment I: Sample I End of Testing—Before Unloading

Figure 26. Experiment I: Sample J Start of Testing—Before Loading

Figure 27. Experiment I: Sample J End of Testing—Before Unloading

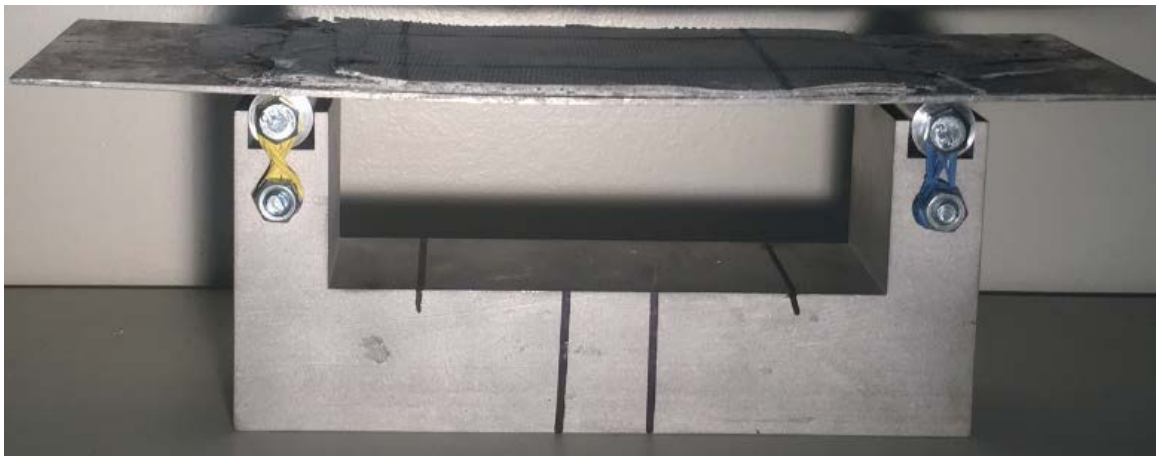

Figure 28. Experiment I: No Permanent Deformation Shown in Sample I

6. Samples K and L

The final pair of tests for Experiment I was conducted with samples K and L. These samples were patched with the wet patching procedure described earlier, but were allowed to cure underwater for four weeks before being taken out and tested. Sample K and L were both patched on the top side of the sample, demonstrating a wet patch in compression. The patch thicknesses for these samples are shown in Table 3 and the maximum load applied during this test is shown in Table 4. Figure 29 shows Sample K at the start of testing, prior to loading and Figure 30 shows Sample K at the end of testing, before unloading. Figure 31 shows Sample L at the start of testing, prior to loading and Figure 32 shows Sample L at the end of testing, before unloading. After the removal of the load, there is no permanent deformation visible but delamination of the patch occurred and is visible. This is shown in Figure 33.

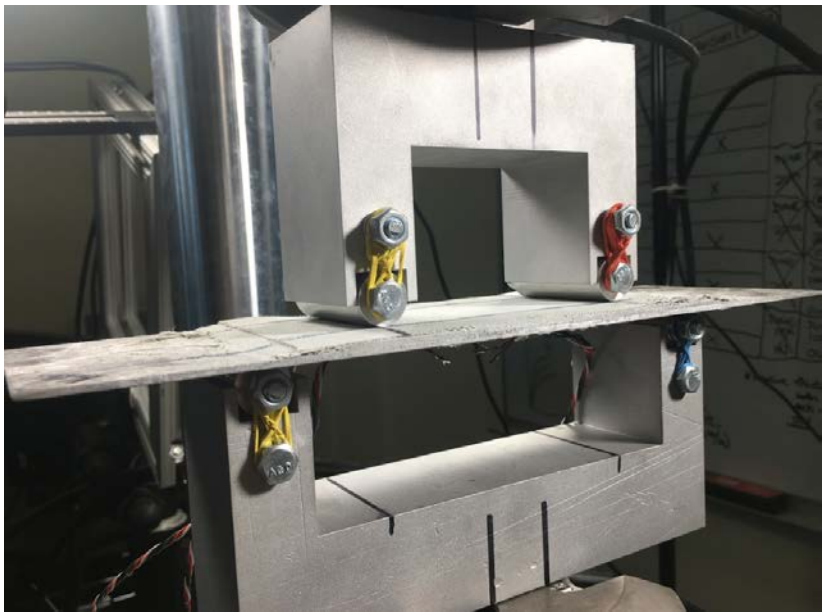

Figure 29. Experiment I: Sample K Start of Testing-Before Loading

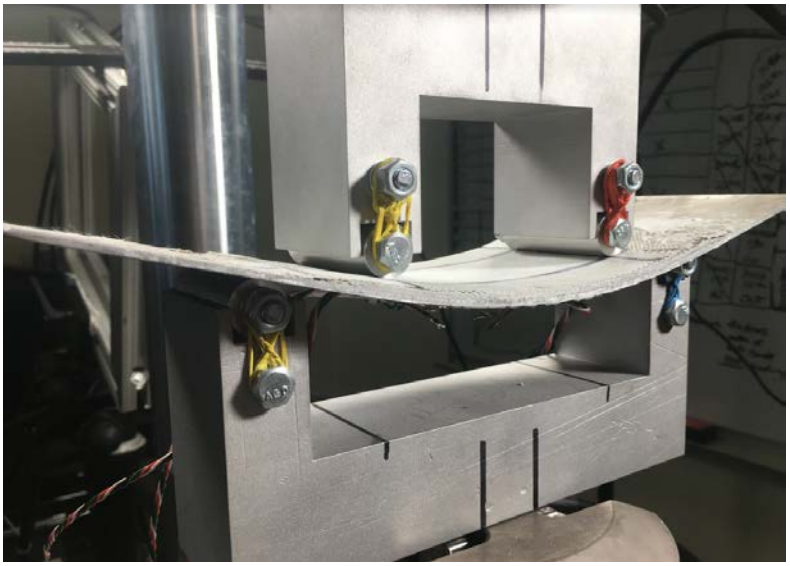

Figure 30. Experiment I: Sample K End of Testing-Before Unloading

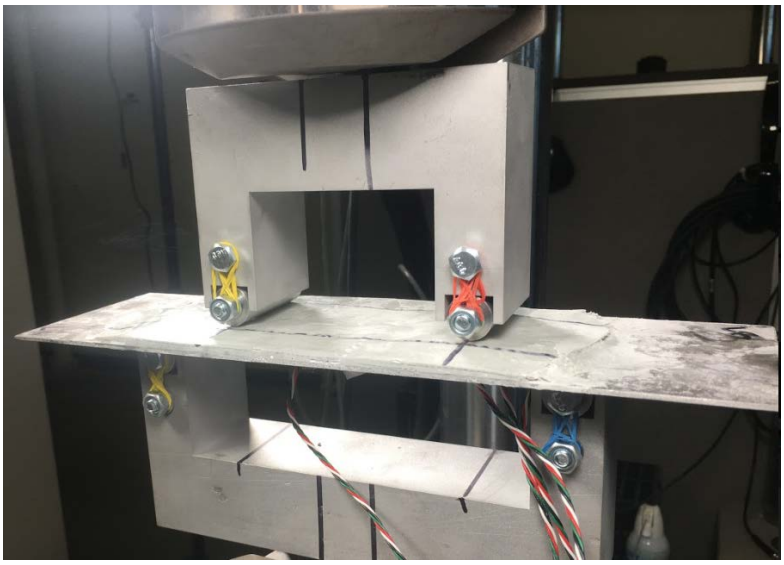

Figure 31. Experiment I: Sample L Start of Testing-Before Loading

Figure 32. Experiment I: Sample L End of Testing-Before Unloading

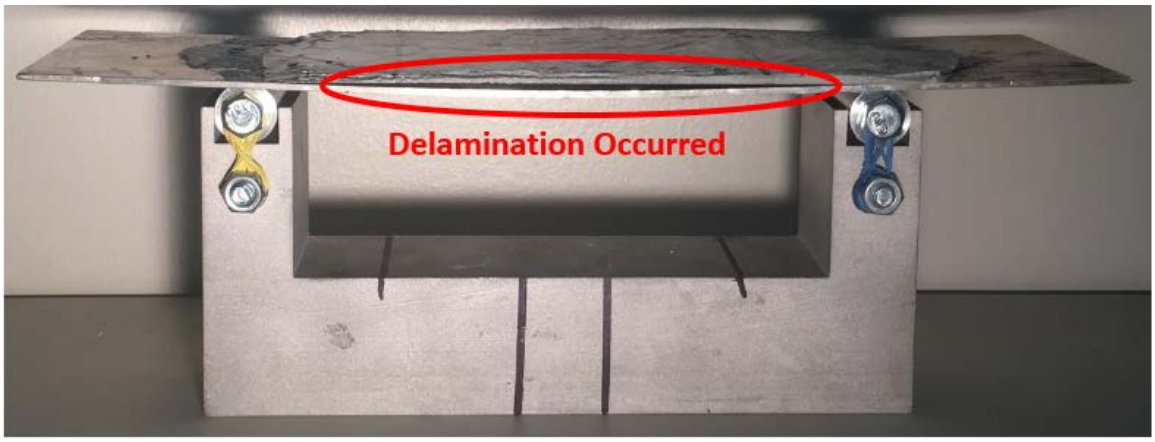

Figure 33. Experiment I: No Permanent Deformation Shown, but Delamination Occurred in Sample K

C. EXPERIMENT II: TENSILE TESTING

For the tensile test conducted on all samples in Experiment II, the INSTRON 5980 Series machine was used as the primary testing equipment, shown in Figure 34. The INSTRON 5982 dual column floor frame model, using the Bluehill Universal Version 4.03 program, has a maximum loading of 100 kN [16]. For each sample in the test matrix of Experiment II shown in Table 2, four uniaxial strain gauges were applied to measure the longitudinal strain at various locations of the samples as shown in Appendix C. The placement of these strain gauges were chosen to ensure the region around the hole would be properly captured as load increases during the testing. The uniaxial strain gauges were Omega part number SGD-7/350-LY11. The INSTRON test procedure was set to start at zero mm of displacement and load at a rate of 1mm/min until 5mm ± 0.5 mm was reached to ensure the sample being tested was loaded past the elastic region. The thickness of the patches for each sample are shown in Table 5.

Figure 34. Experiment II Testing Equipment: INSTRON 5082

Table 5. Experiment II Samples A–L Patch Thicknesses

Experiment II: Tension Test	
Sample	Patch Thickness [m]
A	N/A
B	N/A
C	0.00307
D	0.00298
E	0.00337
F	0.00298
G	0.00313
H	0.00333
I	0.00335
J	0.00333
K	0.00333
L	0.00314

1. Samples A and B

The first two samples of Experiment II were the samples A and B, the samples without patches. Figure 35 shows Sample A, prior to loading. Figure 35 also represents all Samples in Experiment II prior to loading.

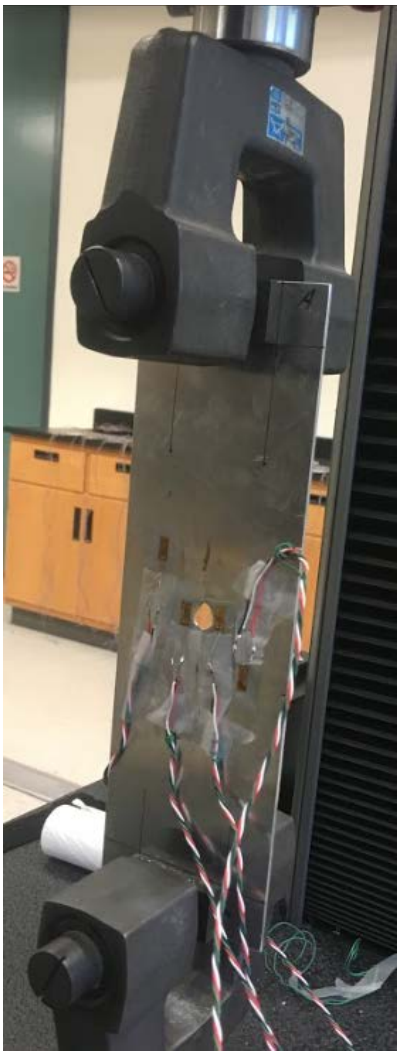

Figure 35. Experiment II: Sample A Start of Testing—Before Loading

2. Samples C and D

The next pair of testing was conducted with samples C and D. These Samples were patched with the dry patching procedure described earlier, but were allowed to cure above the water in a dry environment. The patch thicknesses for these samples are shown in Table 5.

3. Samples E and F

The next pair of testing was conducted with samples E and F. These Samples were patched with the wet patching procedure described earlier, but were allowed to cure

underwater for 24 hours before being taken out and tested. The patch thicknesses for these samples are shown in Table 5.

4. Samples G and H

The next pair of testing was conducted with samples G and H. These Samples were patched with the wet patching procedure described earlier, but were allowed to cure underwater for one week before being taken out and tested. The patch thicknesses for these samples are shown in Table 5.

5. Samples I and J

The next pair of testing was conducted with samples I and J. These Samples were patched with the wet patching procedure described earlier, but were allowed to cure underwater for two weeks before being taken out and tested. The patch thicknesses for these samples are shown in Table 5.

6. Samples K and L

The final pair of testing for Experiment II was conducted with samples K and L. These Samples were patched with the wet patching procedure described earlier, but were allowed to cure underwater for four weeks before being taken out and tested. The patch thicknesses for these samples are shown in Table 5.

D. COMPUTER MODELING

Finite element analysis (FEA) played an important role in the development of Experiments I and II. FEA provided an analysis of the effects of a hole on the aluminum sample under a four point loading condition and a purely axial loading condition.

1. Experiment I: Four-Point Bending Test FEA Modeling

The first objective of using FEA was to conduct preliminary modeling of the aluminum samples with holes being used in the Experiment I, and loading the modeled sample to determine the specific load that would result in a bending stress equal to that of the material's yield stress given by the mechanical properties shown in Table 1. The

solution of the FEA is shown in Figure 36. The next objective was to calculate the maximum stress experienced at the hole and use to estimate the stress concentration factor (SCF) caused by the hole. With the SCF estimated from computer modeling, the load in which to use as a baseline for the MTS machine for Experiment I was determined. This load was calculated using the FEA to ensure the region around the hole, between the top loading points, would transition into the material's plastic region if no patch was used in Experiment I.

A computer model of the sample with the dimensions shown in Figure 3 and Table 1 was created and imported into ANSYS Mechanical Workbench for FEA analysis. The FEA model was constructed so as to produce the boundary conditions that the sample would be subjected to in Experiment I. The top portion of the four point testing device shown in Figure 5 makes contact two inches (.0508m) from the hole's center on both sides and is two inches (.0508m) in width. A downward (-Y) force is added along both sides of the hole at the contact area of the top device.

The initial force used to load the model was calculated using the aluminum's yield stress. The amount to load the model to ensure the 4 inches (.1016 m) by 4 inches (.1016 m) area between the top loading rollers would transition into the plastic region, the following process was used to set the final loading criteria to 643N:

1. Find the load that will equal a bending stress of σ_y using the following equation for bending stress: $\sigma_y = \frac{My}{I}$; where $M = Force\ x\ Moment\ arm$, $y = \frac{thickness\ of\ material\ (t)}{2}$, and I is Moment of Inertia (Izz), $I_{zz} = \frac{b*t^3}{12}$.

2. Given 5052 aluminum yield strength; $\sigma_y = 180MPa$ the force is calculated to equal 643N.

3. The FEA model was loaded to 643 N.

The Sample was subjected to a ramped force over 10 time steps starting at 0 N and increasing to 643 N at equal intervals.

The baseline results using ANSYS Mechanical Workbench for the loading condition of 643 N are shown in Figure 36. All results using ANSYS Mechanical Workbench are a result of ensuring the material data input for metal plasticity was incorporated in the analysis. A Bilinear Isotropic Hardening condition was used, assuming the yield surface expands uniformly during plastic deformation. As shown, the maximum stress (σ_{max}) experienced is 302 MPa. From the Stress Concentration Factor Equation: $K_t = \frac{\sigma_{max}}{\sigma_{nominal}}$, the stress concentration was calculated using ANSYS to equal 1.677. To validate and compare ANSYS simulation of the aluminum sample, a chart of Theoretical Stress-Concentration Factors [17], shown in Figure 37, was used. Using the dimensions in Table 1, the following variables were calculated and plotted on Figure 31: $\frac{d}{w} = .125$ and $\frac{d}{h} = 6.25$. The theoretical stress concentration factor, K≈ 1.7, agrees with ANSYS modeling and simulation.

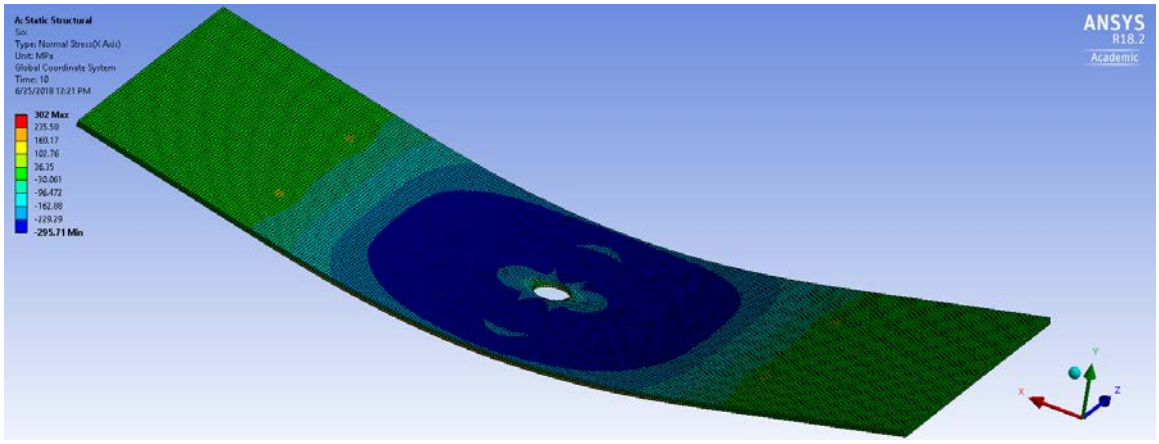

Figure 36. FEA Solution: Maximum Stress without Patch, σ_{max}=302MPa

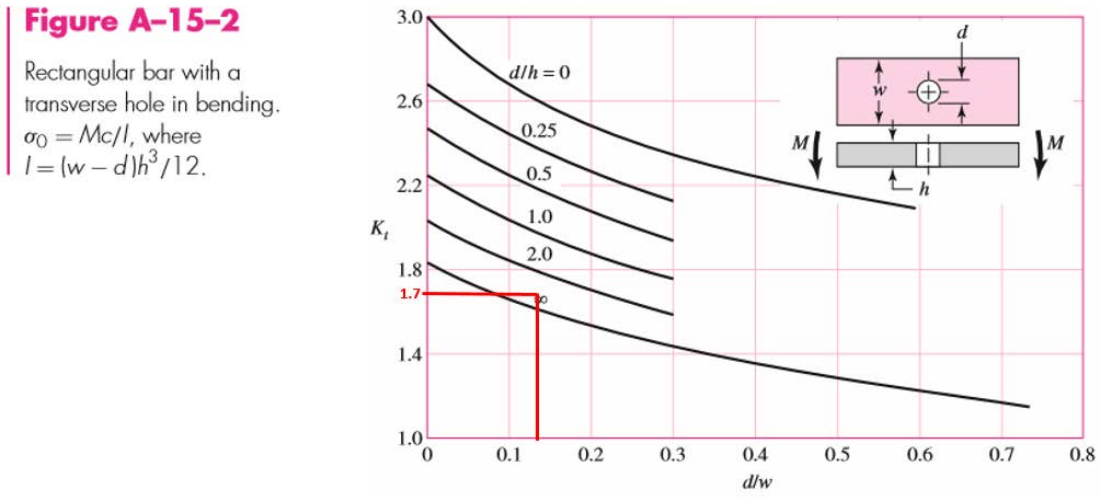

Figure 37. Theoretical Stress-Concentration Factor, K=1.7. Adapted from [17].

The second objective using FEA was to conduct modeling of the aluminum samples with a composite repair patch being used in Experiment I. Each composite repair patch was modeled using initial tensile testing data and the resulting material properties-Modulus of Elasticity and the Poisson's ratio. The FEA was conducted to simulate the four-point bending test that would be conducted in Experiment I. The stress and strain data located at the hole and away from the hole was used in the Analysis and Results section of this thesis to compare the FEA model and the Experimental testing conducted. The four-point bending FEA model was also used to derive a theoretical strain concentration factor that would be used for calculating the concentrated bending stress of each sample with patches. One solution of the FEA is shown in Figure 37, which uses the material properties of Sample C for the patch modeling.

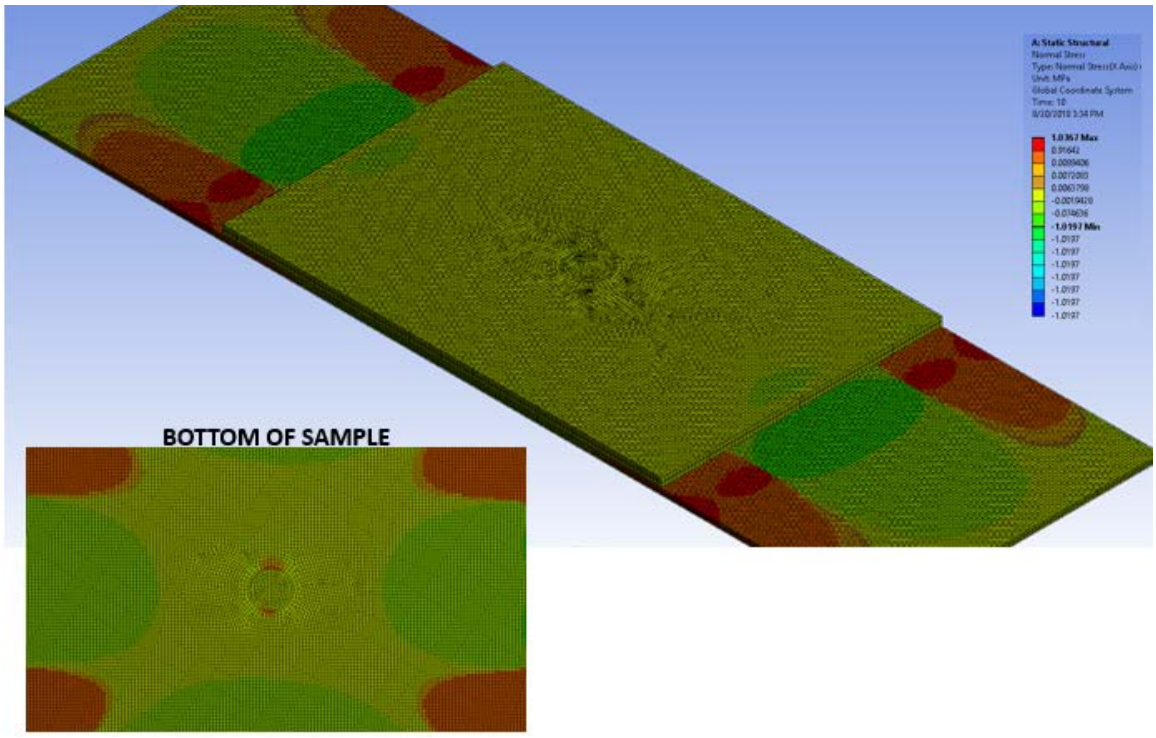

Figure 38. FEA Solution Experiment I-Sample C

2. Experiment II: Tensile Test FEA Modeling

A computer model of the sample with the dimensions shown in Figure 3 and Table 1 was created and imported into ANSYS Mechanical Workbench for FEA analysis. The FEA model was constructed so as to produce the boundary conditions that the sample would be subjected to in Experiment II. The Sample was subjected to a 13000 N force in the positive X direction (+x) along both sides of the end of the sample (26,000 N force total). This models the Experiment II machine device that clamps and holds each sample during the tensile test. At the other end of the sample, a boundary condition of zero displacement was assigned.

The Sample was subjected to a ramped force over 10 time steps starting at 0 N and increasing to 26,000 N at equal intervals. The solution of the FEA model which models Sample A and B is shown in Figure 38.

All results using ANSYS Mechanical Workbench are a result of ensuring the material data input for metal plasticity was incorporated in the analysis. A Bilinear

Isotropic Hardening condition was used, assuming the yield surface expands uniformly during plastic deformation. Shown in Figure 39 as red contour coloring, the maximum stress (σ_{max}) experienced is 430.2 MPa. From the Stress Concentration Factor Equation:$K_t = \frac{\sigma_{max}}{\sigma_y}$, where σ_y is the aluminum sample's yield stress, $\sigma_y = 180\ MPa$, the stress concentration was calculated using ANSYS to equal 2.39. To validate and compare ANSYS simulation of the aluminum sample, a chart of Theoretical Stress-Concentration Factors [17], shown in Figure 40, was used. Using the dimensions in Table 1 the following variables were calculated and plotted on Figure 40: $\frac{d}{w} = .125$. The theoretical stress concentration factor derived from chart is K≈ 2.62. The numerical vs. analytical stress concentration factors are shown to be within 10% of each other, proving the numerical model created in ANSYS is comparable to actual experimentation.

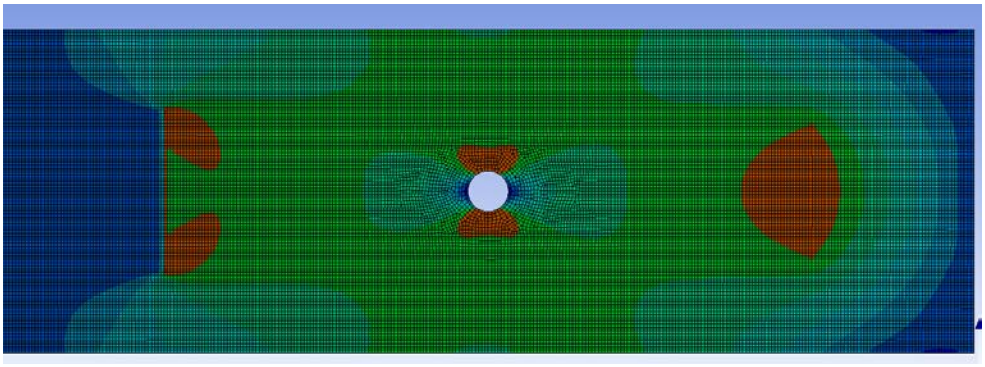

Figure 39. FEA Solution: Experiment II-Sample A

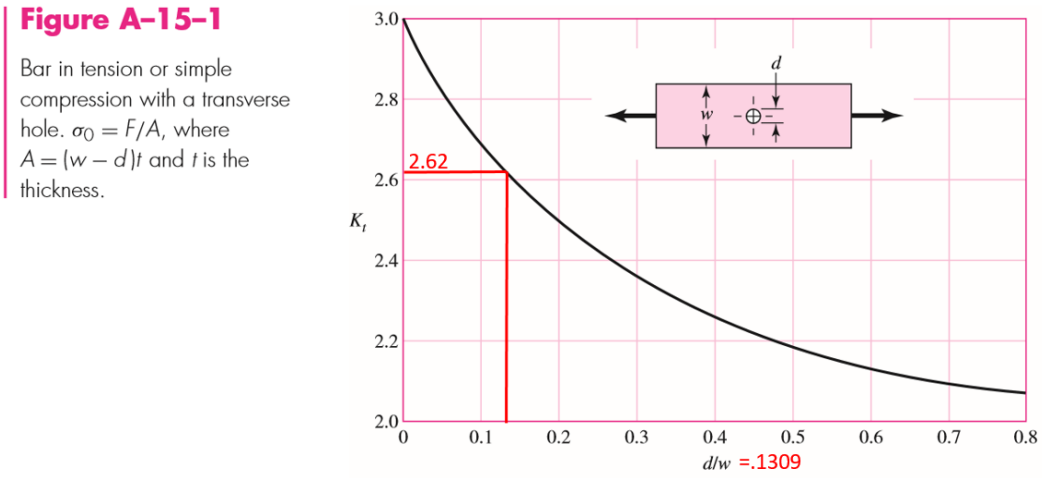

Figure 40. Theoretical Stress-Concentration Factor, K=2.62. Adapted from [17].

The second objective using FEA for Experiment II was to conduct modeling of the aluminum samples a composite repair patch being used in the Experiment II. The composite repair patch was modeled using initial tensile testing data and the resulting material properties, such as the Modulus of Elasticity and the Poisson's ratio. The FEA was conducted to simulate the tensile test that would be conducted in Experiment II. The stress and strain data located at the hole and away from the hole was used in the Analysis and Results section of this thesis to compare the FEA model and the experimental testing conducted. The tensile test FEA model was also used to derive a theoretical stress concentration factor that would be used for calculating the concentrated axial stress of each sample with patches. One solution of the FEA is shown in Figure 41, which uses the material properties of Sample C for the patch modeling.

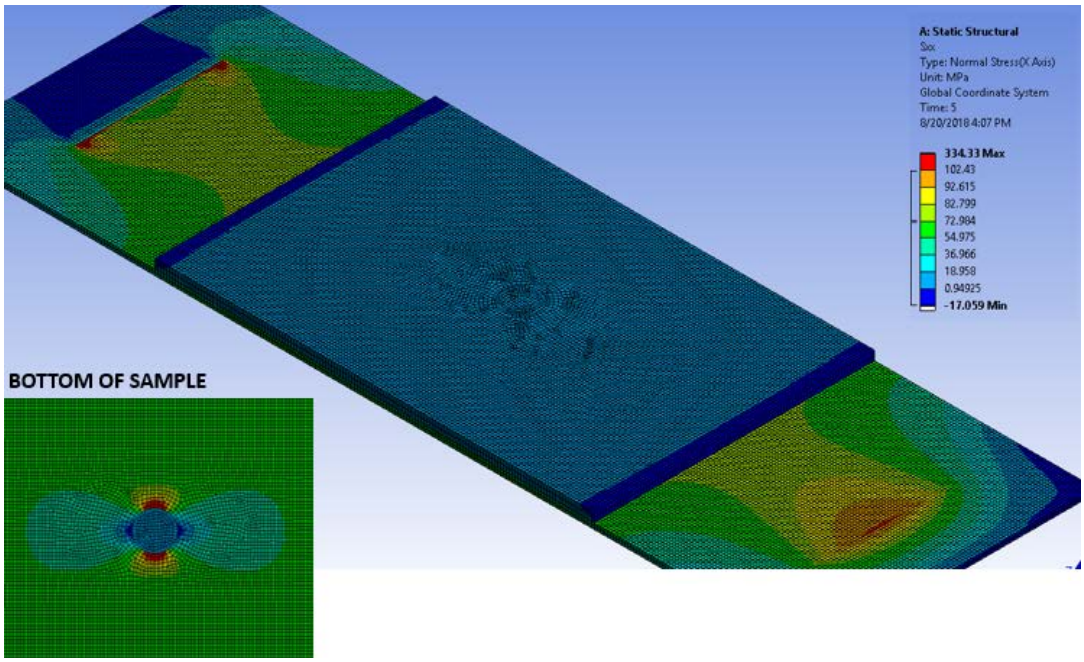

Figure 41. FEA Solution: Experiment II- Sample C

III. ANALYSIS AND RESULTS

A. PRELIMINARY CALCULATIONS

Before the mechanical behavior of each sample in the two experiments conducted is presented, the following discussion is provided to enhance the reader's understanding of the mechanical behavior of a single layer of the eight layer patch used in this thesis research.

To begin with, it is assumed that the bonding between each of the eight layer fibers and the epoxy of each sample patch was bonded perfectly. Therefore, the strain of the fibers and the strain of the epoxy are equal in the axial loading direction (direction of 1 in Figure 42). (i.e.,$\varepsilon_{fiber} = \varepsilon_{epoxy} = \varepsilon_1$) when the layered patch is subjected to a uniaxial force along the fiber direction or when analyzing the stress along the fiber direction. This is shown in Figure 42 [18].

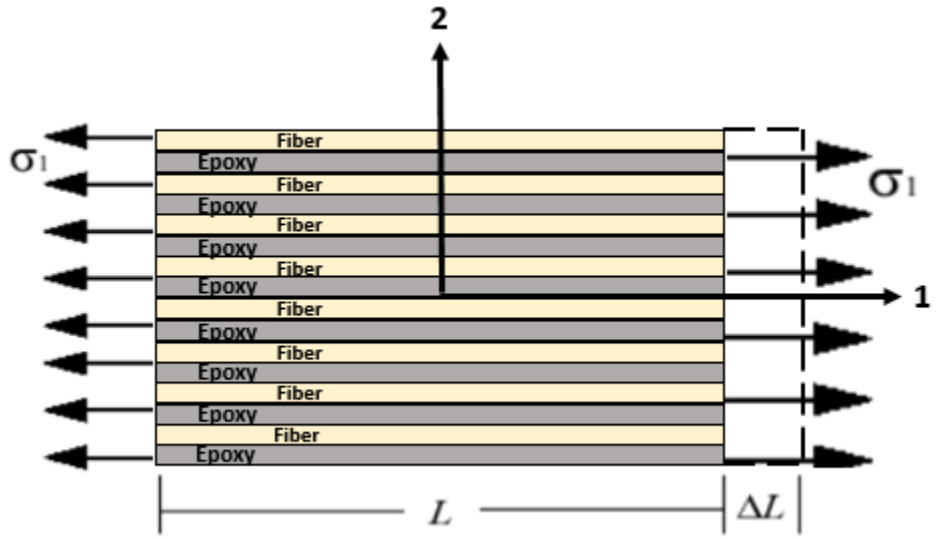

Figure 42. Fiber and Epoxy Patch Diagram. Adapted from [17].

The total force applied on the layer is

$$P_1 = \sigma_1 A_1 = \sigma_f A_f + \sigma_e A_e,$$

where A_f and A_e are the cross section areas of the fibers and the epoxy. The Modulus of elasticity, E_{patch} , is written as

$$E_{patch} = \frac{\sigma_1}{\varepsilon_1} = \frac{P_1/A_1}{\varepsilon_1} = \frac{\sigma_f A_f + \sigma_e A_e}{A_1 \varepsilon_1} = \frac{\sigma_f A_f L}{\varepsilon_1 A_1 L} + \frac{\sigma_e A_e L}{\varepsilon_1 A_1 L}$$

$$E_{patch} = E_{fiber} Vf_{fiber} + E_{epoxy} Vf_{epoxy}\ , \qquad (1)$$

where Vf is the volume fraction and L is the length of the layer. Note: $Vf_f + Vf_e = 1$ based on non-void assumption. [18]

The major Poisson's ratio, ν, of each sample can be defined as

$$\nu_{patch} = -\frac{\varepsilon_2}{\varepsilon_1}.$$

As shown in the calculation of E_{patch} section, $\varepsilon_f = \varepsilon_e = \varepsilon_1$, and the traverse strain is the sum of the contribution from the fibers and the epoxy, which are proportional to their respective volume functions [18]

$$\varepsilon_2 = V_{ff}\varepsilon_f + V_{fe}\varepsilon_e = -(Vf_f \varepsilon_f \nu_\nu + Vf_e \varepsilon_e \nu_e).$$

The major Poisson's ratio can be written as

$$\nu_{patch} = -\frac{\varepsilon_2}{\varepsilon_1} = \frac{Vf_f \varepsilon_f \nu_\nu}{\varepsilon_f} + \frac{Vf_e \varepsilon_e \nu_e}{\varepsilon_e}$$

$$\nu_{patch} = \nu_{fiber} Vf_{fiber} + \nu_{epoxy} Vf_{epoxy}\ . \qquad (2)$$

Equation (1) and Equation (2) are the final equations used to calculate the modulus of elasticity and Poisson's ratio of each sample. The volume fractions of both the fiber (Vf_f) and the epoxy (Vf_e) are measured from each sample. The two unknowns in each Equation are the E_{fiber} , E_{epoxy} in Equation (1) and the ν_{fiber}, ν_{epoxy} in Equation (2). It is necessary to solve for these four unknowns so as to use Equation (1) and Equation (2) for all samples.

All four samples were solved for using the experimental data collected from two ASTM standard tensile tests on a composite sample. Table 6 exhibits the tensile testing data of two samples used in the Equations shown in Figure 43 and Figure 44 to derive the four unknown values in Equation (1) and (2) [19].

Table 6. Composite Samples 1 and 2 Tensile Test Data

Sample	Thickness (m)	Width (m)	Area (m^2)	Single Ply Thickness (m)	All 8 Ply Thickness (m)	Epoxy Thickness (m)	Vf Plies	Vf Epoxy	Ecomp (GPa)	vComp
1	1.94E-03	2.03E-02	3.93E-05	2.03E-04	1.63E-03	3.11E-04	25.18%	74.82%	54.75	3.26E-01
2	1.96E-03	2.03E-02	5.88E-05	2.03E-04	1.63E-03	3.30E-04	24.93%	75.07%	53.89	4.40E-04

$$E_{comp} = E_{fiber} \cdot Vf_{fiber} + E_{epoxy} \cdot Vf_{epoxy}$$

$$E_{compA} = E_{fiber} \cdot Vf_{fiberA} + E_{epoxy} \cdot Vf_{epoxyA}$$

$$E_{compB} = E_{fiber} \cdot Vf_{fiberB} + E_{epoxy} \cdot Vf_{epoxyB}$$

$$\begin{Bmatrix} E_{compA} \\ E_{compB} \end{Bmatrix} = \begin{bmatrix} Vf_{fiberA} & Vf_{epoxyA} \\ Vf_{fiberB} & Vf_{epoxyB} \end{bmatrix} \begin{Bmatrix} E_{fiber} \\ E_{epoxy} \end{Bmatrix}$$

$$\begin{Bmatrix} E_{fiber} \\ E_{epoxy} \end{Bmatrix} = \begin{bmatrix} Vf_{fiberA} & Vf_{epoxyA} \\ Vf_{fiberB} & Vf_{epoxyB} \end{bmatrix}^{-1} \begin{Bmatrix} E_{compA} \\ E_{compB} \end{Bmatrix}$$

$$\begin{Bmatrix} E_{fiber} \\ E_{epoxy} \end{Bmatrix} = \frac{1}{\left(Vf_{fiberA} \cdot Vf_{epoxyB} - Vf_{epoxyA} \cdot Vf_{fiberB}\right)} \begin{bmatrix} Vf_{epoxyB} & -Vf_{epoxyA} \\ -Vf_{fiberB} & Vf_{fiberA} \end{bmatrix} \begin{Bmatrix} E_{compA} \\ E_{compB} \end{Bmatrix}$$

Figure 43. Equations Used to Derive the Two Unknowns in Equation 1. Adapted from [19].

$$\nu_{comp} = \nu_{fiber} \cdot Vf_{fiber} + \nu_{epoxy} \cdot Vf_{epoxy}$$

$$\nu_{compA} = \nu_{fiber} \cdot Vf_{fiberA} + \nu_{epoxy} \cdot Vf_{epoxyA}$$

$$\nu_{compB} = \nu_{fiber} \cdot Vf_{fiberB} + \nu_{epoxy} \cdot Vf_{epoxyB}$$

$$\begin{Bmatrix} \nu_{compA} \\ \nu_{compB} \end{Bmatrix} = \begin{bmatrix} Vf_{fiberA} & Vf_{epoxyA} \\ Vf_{fiberB} & Vf_{epoxyB} \end{bmatrix} \begin{Bmatrix} \nu_{fiber} \\ \nu_{epoxy} \end{Bmatrix}$$

$$\begin{Bmatrix} \nu_{fiber} \\ \nu_{epoxy} \end{Bmatrix} = \begin{bmatrix} Vf_{fiberA} & Vf_{epoxyA} \\ Vf_{fiberB} & Vf_{epoxyB} \end{bmatrix}^{-1} \begin{Bmatrix} \nu_{compA} \\ \nu_{compB} \end{Bmatrix}$$

$$\begin{Bmatrix} \nu_{fiber} \\ \nu_{epoxy} \end{Bmatrix} = \frac{1}{\left(Vf_{fiberA} \cdot Vf_{epoxyB} - Vf_{epoxyA} \cdot Vf_{fiberB}\right)} \begin{bmatrix} Vf_{epoxyB} & -Vf_{epoxyA} \\ -Vf_{fiberB} & Vf_{fiberA} \end{bmatrix} \begin{Bmatrix} \nu_{compA} \\ \nu_{compB} \end{Bmatrix}$$

Figure 44. Equations Used to Derive the Two Unknowns in Equation 2. Adapted from [19].

From the Equations shown in Figure 43 and Figure 44, the fiber's and epoxy's moduli of elasticity and Poisson's ratios are calculated and these values were used in Equations (1) and (2) to derive the modulus of elasticity and Poisson's ratios for each of the composite patches for the different sample tests in Experiment I and Experiment II described in future chapters. Table 7 shows the Modulus of Elasticity and Poisson's ratio derived from these Equations for each test sample in Experiments I and II. The typical E glass fiber Modulus of Elasticity is 80 GPa [20]. The E Glass fiber used in this thesis has a modulus of elasticity that is approximately 38.12% less than typical E Glass with the following composition: SiO_2 54wt%, Al_2O_3 14wt%, CaO+MgO 22wt%, B_2O_3 10wt% and Na_2O+ K_2O less then 2wt% [20].

Table 7. Modulus Of Elasticity and Poisson's Ratio of All Samples

	SAMPLE	Patch Thickness	E_patch [Gpa]	v_patch
Experiment 1	A	N/A	N/A	N/A
	B	N/A	N/A	N/A
	C	0.00366395	56.12730755	0.2658124
	D	0.00365125	56.135357	0.2660366
	E	0.0027432	56.90406992	0.2874469
	F	0.00255905	57.12649765	0.2936419
	G	0.00321945	56.44682457	0.2747116
	H	0.0032004	56.46250156	0.2751483
	I	0.0027432	56.90406992	0.2874469
	J	0.00338455	56.31834979	0.2711333
	K	0.0032258	56.44164006	0.2745672
	L	0.0032004	56.46250156	0.2751483
Experiment 2	A	N/A	N/A	N/A
	B	N/A	N/A	N/A
	C	0.00306705	56.5776933	0.2783566
	D	0.0029845	56.65416102	0.2804864
	E	0.0033655	56.33253049	0.2715283
	F	0.00297815	56.66021873	0.2806551
	G	0.00313055	56.52161619	0.2767947
	H	0.00333375	56.35652515	0.2721966
	I	0.0033528	56.34207382	0.2717941
	J	0.00333375	56.35652515	0.2721966
	K	0.00333375	56.35652515	0.2721966
	L	0.00314325	56.51067265	0.2764899

B. EXPERIMENT I: FOUR-POINT BENDING TEST

The four-point bending test analysis and calculations are treated as a composite beam formed from two materials, Aluminum and Composite Patch. The stress and strain is a linear function through the thickness for each material section of the beam [2]. The bending stress Equation shown in Equation (3) requires the location of the neutral axis (y) to be calculated appropriately.

$$\sigma_{bending} = \frac{My}{I} \tag{3}$$

For single material beams, the neutral axis (NA) is located at the centroid of the cross section of the material. For composite beams, this is not the case. The location of the NA must be calculated before the bending stress can be solved for. The location of the NA is a function of the relative stiffness and the geometry of each of the material sections of the beam. The NA location for each sample in Experiment I was assigned to be relative to the bottom surface of the beam. The diagram for the NA derivation given in Equation (4) is shown in Figure 45

$$\mathrm{Y}_{Bar} = \frac{Y_{bar1}A_1E_1 + Y_{bar2}A_2E_2}{A_1E_1 + A_2E_2}, \tag{4}$$

where

Y_{bar1}=thickness of Aluminum Sample + ½ thickness of the Composite patch.

Y_{bar2}= ½ thickness of the Aluminum Sample.

A_1= patch thickness x patch width.

A_2=plate thickness x plate width.

E_1=Modulus of Elasticity of Composite Patch derived from earlier.

E_2=Modulus of Elasticity of 5052-H32 Sample

Each sample in Experiment I is modeled by a composite beam made of two different materials. Each material has a different moment of inertia. The moment of inertia for the entire beam is derived using the parallel axis theorem. Equation (5) displays the Equation derived used for each Sample.

$$\mathrm{I}_{Bar} = \frac{1}{12}wt_2{}^3 + wt_2(Y_{Bar} - \frac{t_2}{2})^2 + \frac{1}{12}wt_1{}^3 + nwt_1(Y_{Bar} - t_1 - \frac{t_1}{2})^2 \tag{5}$$

The ratio n is given by

$$n = \frac{Modulus\ of\ Elasticity\ for\ Composite\ Patch}{Modulus\ of\ Elasticity\ for\ Aluminum} = \frac{E_1}{E_2}.$$

Table 8 displays the values of Y_{Bar}, $I_{Bar,}$ and the ratio n $_{for}$ all samples in Experiment I. These were used in calculating the bending stress in each test of Experiment I.

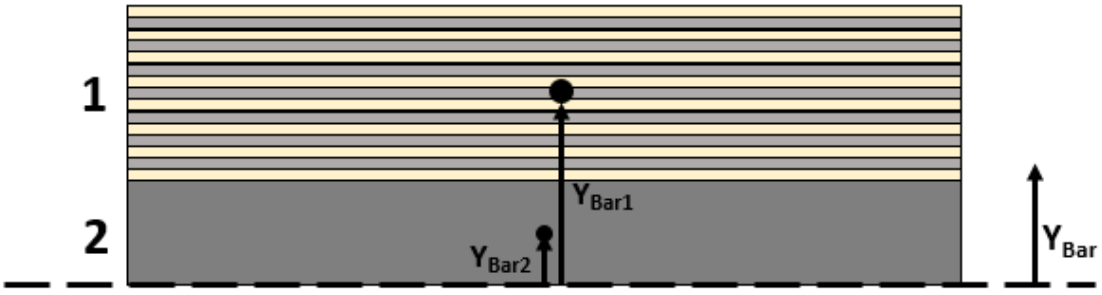

Figure 45. Neutral Axis Diagram

Table 8. Samples C-L Neutral Axis and Modulus of Elasticity Values

Sample	YBAR FOR SAMPLE (m)	I BAR (m^4)	n=E1/E2
C	1.2879E-03	8.39E-10	0.06
D	1.2784E-03	8.30E-10	0.06
E	1.1955E-03	3.77E-10	0.06
F	1.1800E-03	3.15E-10	0.06
G	1.2414E-03	5.82E-10	0.06
H	1.2396E-03	5.72E-10	0.06
I	1.1781E-03	3.75E-10	0.06
J	1.2351E-03	6.68E-10	0.06
K	1.2392E-03	5.85E-10	0.06
L	1.2396E-03	5.72E-10	0.06

The results to follow were calculated using the following formulas with the load recorded from the MTS machine

$$\sigma_{B1} = \frac{nM(t-Y_{Bar})}{I_{Bar}} \quad (6)$$

$$\sigma_{B2} = \frac{MY_{Bar}}{I_{Bar}}, \quad (7)$$

where σ_{B1} is the nominal stress carried by the Composite Patch, σ_{B2} is the nominal stress carried by the Aluminum Sample and M is the moment created from the half load of the MTS machine times the moment arm (.0381m). In addition, $t = t_1 + t_2$.

The concentration factor used to calculate the concentrated stress due to the hole in the Aluminum Sample was derived from the FEA model and used on each sample. Equations (8) shows the equation used in Experiment I's concentrated stress calculations, where the concentration factor was derived by using the strain measured at the hole and the strain measured away from the hole. Since strain and stress are related by Hooke's law, the concentration factor can be used in calculating the concentrated stress. K is defined in Equation (9).

$$\sigma_{B2} = K[\frac{nMy_{Bar}}{I_{Bar}}] \tag{8}$$

$$K = \frac{\varepsilon_{Hole}}{\varepsilon_{Away\ from\ Hole}} \tag{9}$$

1. Samples A and B

The experimental results of Sample A are shown in Figure 46 displaying the strain (at hole) vs. load curve of the samples with no patches. The numerical results of Sample A are shown in Figure 47, displaying the FEA solution of the strain at the sample's hole during the loading condition of 380 N. Comparing the experimental vs. numerical results at the specified loading condition of 380 N there is a 10.67% difference in strain values, shown in Table 9. The yield point in which the elastic region ends occurs at loading condition of 470 N and is shown in Figure 46.

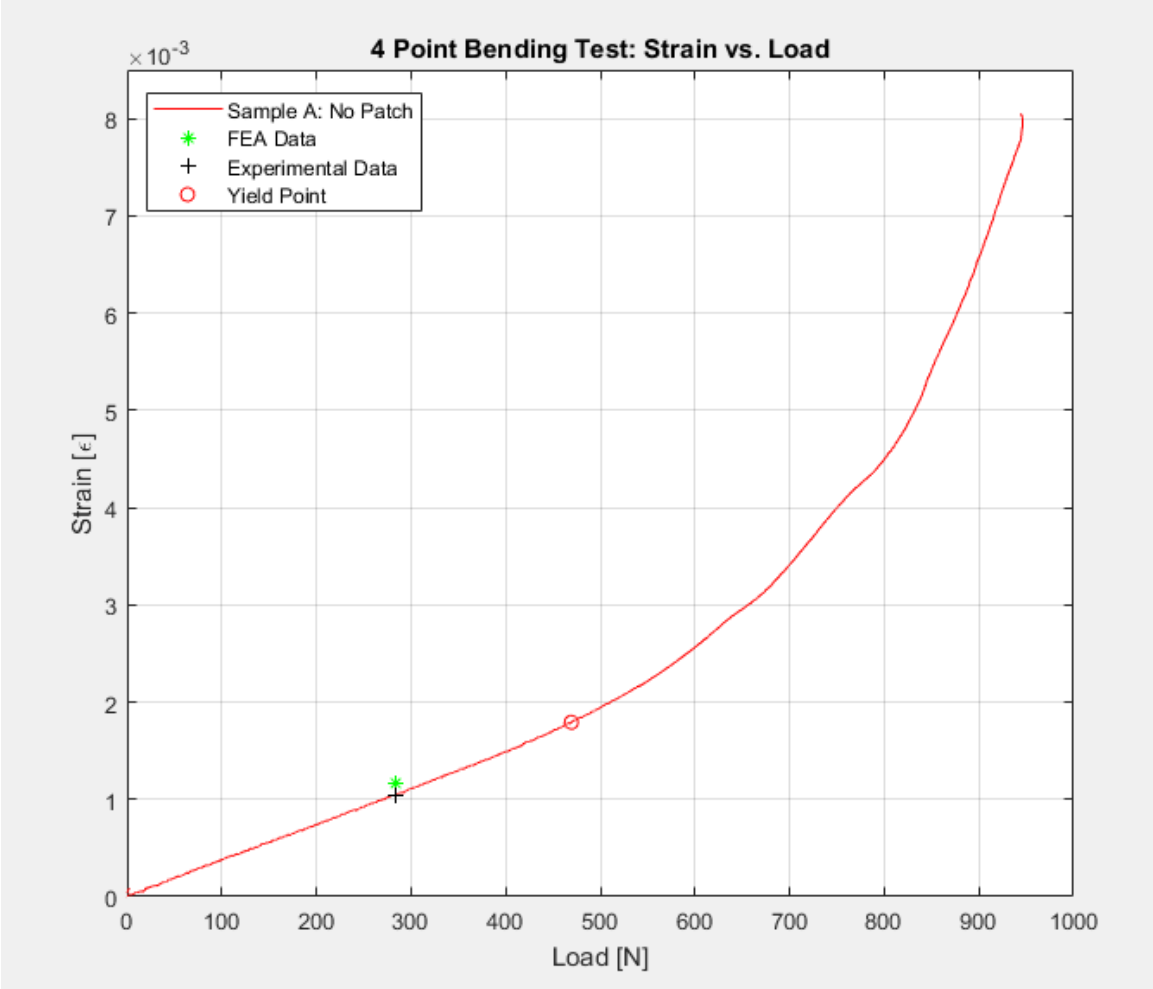

Figure 46. Experiment I: Sample A Strain vs. Load Curve

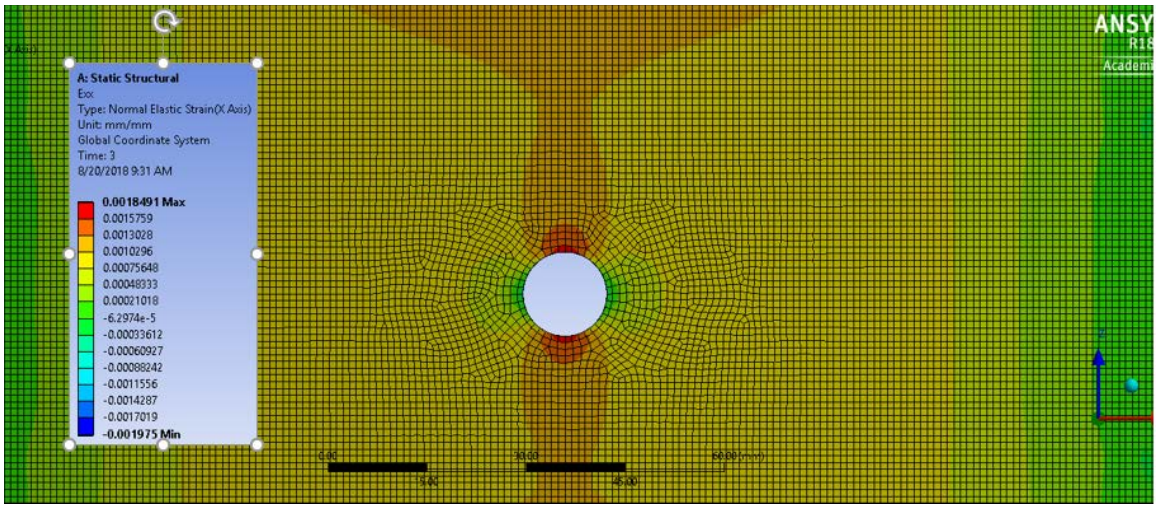

Figure 47. FEA Solution: Sample A at Loading Condition-380 N

Table 9. Sample A: Numerical vs. Experimental Strain Readings at 380 N

	FEA	Experimental
Loading Condition [N]	380	380
Strain Value [με]	1.17	1.048

2. Samples C and D

The experimental results of Sample C are shown in Figure 48 displaying the strain (at hole) vs. load curve of the samples that have been repaired using the dry patching method described earlier. Comparing the experimental results measured from the four point bending test and the numerical results derived from the FEA model, at the specified loading condition of 540 N, there is a 12.73% difference in strain values, shown in Table 10.

The delamination point in which the patch began to physically separate from the aluminum in Experiment I occurred at loading condition of 1070 N and is depicted in Figure 48 as a red circle. Analyzing the numerical data from the FEA at the location shown in Figure 49 and at the specified loading condition of 1070 N, the shear stress and normal stress in the y direction are

$$\tau_{XZ} = .0409\ MPa$$

$$\sigma_Y = 1.36E^{-4}\ MPa.$$

The Shear Stress, τ_{XZ}, is much larger of the two stresses indicating the failure mode of delamination is due to shear stress for Sample C: Dry Patch.

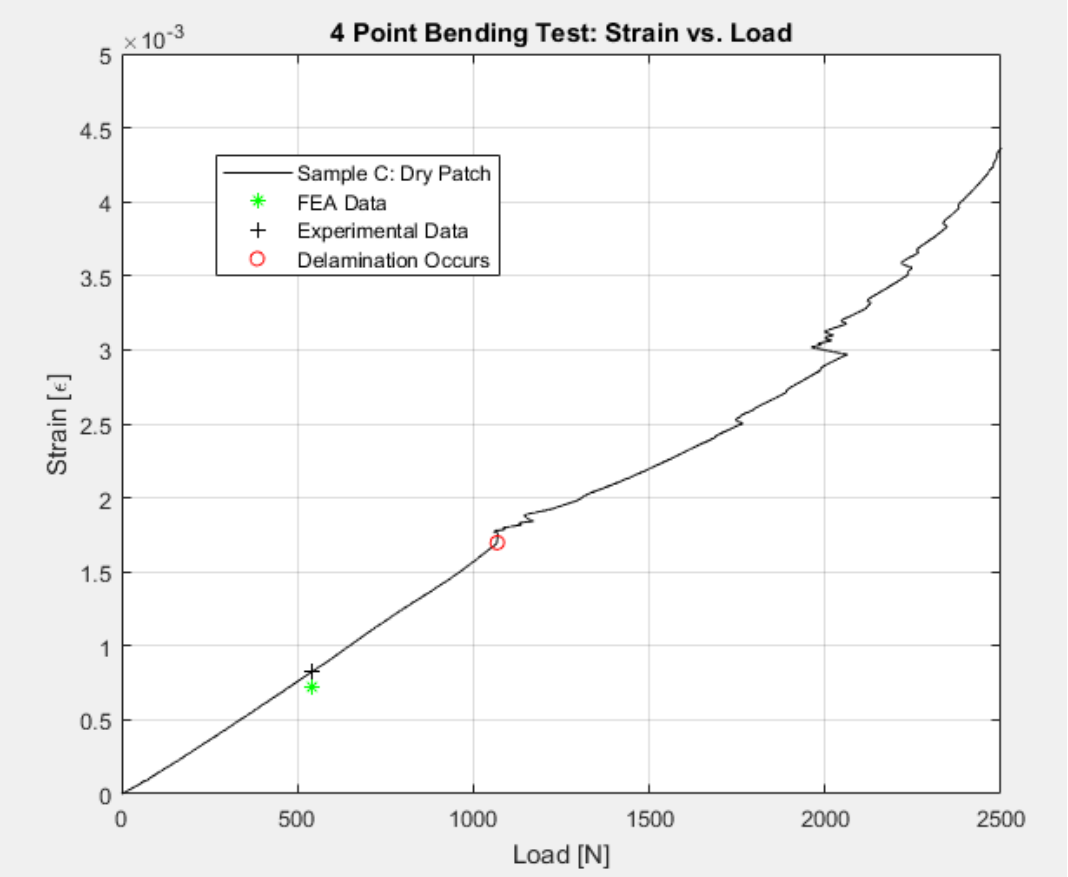

Figure 48. Experiment I: Sample C Strain vs. Load Curve

Table 10. Sample C: Numerical vs. Experimental Strain at 540 N

	FEA	Experimental
Loading Condition [N]	540	540
Strain Value [με]	0.725	0.824

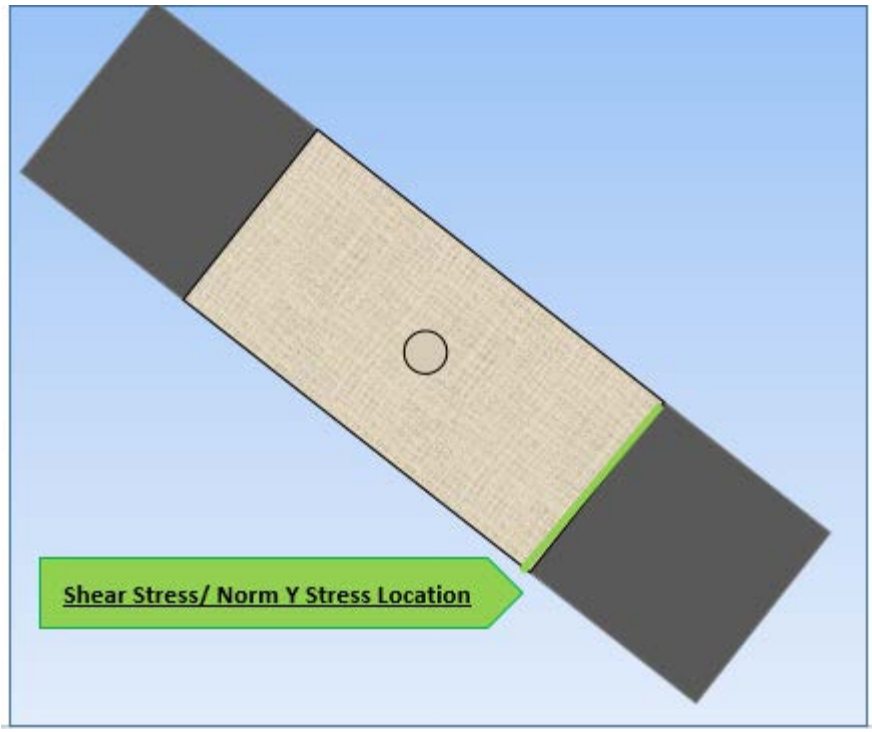

Figure 49. Experiment I: Location of Shear Stress/Norm Y Stress Data Taken for All Samples

3. Samples E and F

The experimental results of Sample E are shown in Figure 50 displaying the strain (at hole) vs. load curve of the samples that have been repaired using the wet patching method described earlier and left in the water to cure for 24 hours. Comparing the experimental results measured from the four point bending test and the numerical results derived from the FEA model at the specified loading condition of 540 N, there is a 6.86% difference in strain values, shown in Table 11.

As shown by the curve displayed in Figure 50, there is no point of delamination, nor does the sample reach a yield point. This specific test sample had a maximum loading condition of 1017 N. Analyzing the strain vs. load curve of Sample A in Figure 46, Sample A has been loaded significantly past its yield point at 1017 N.

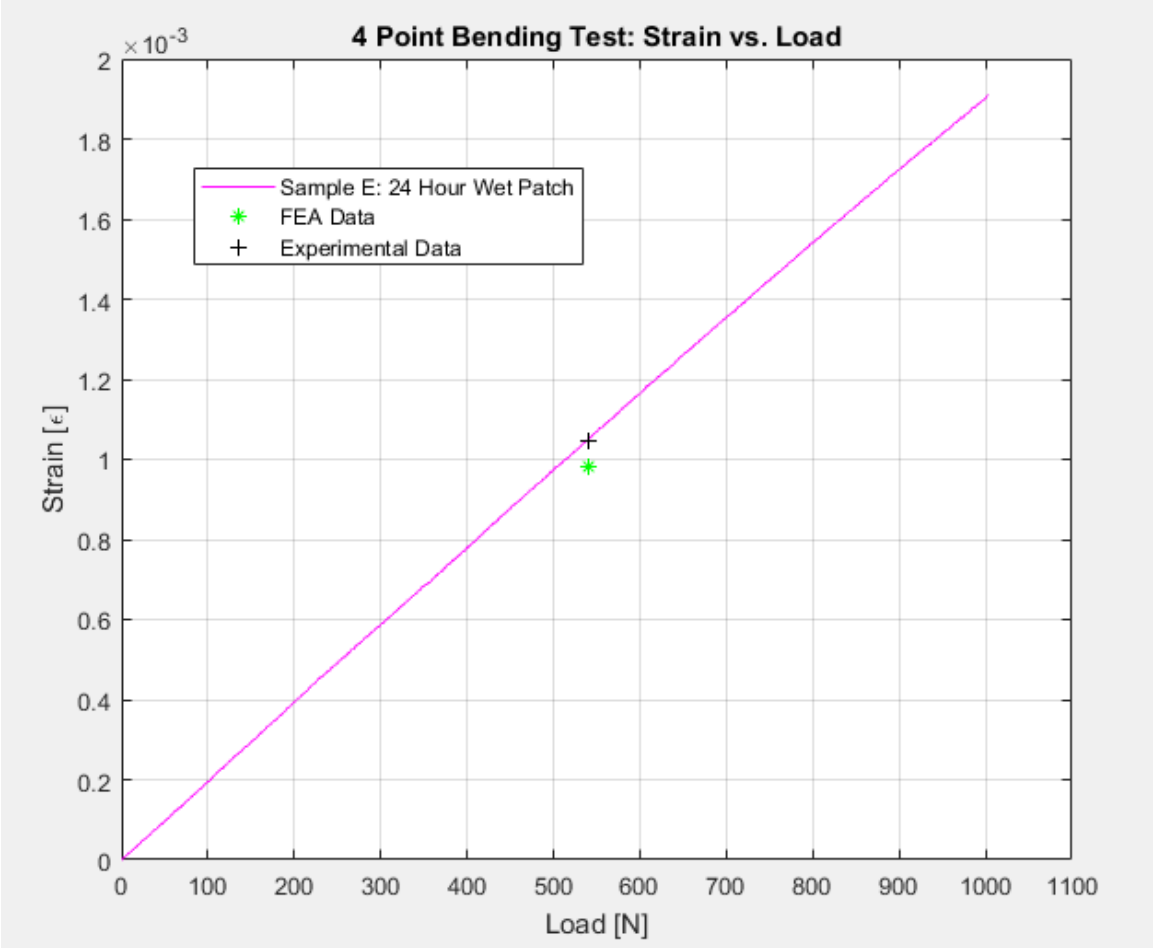

Figure 50. Experiment I: Sample E Strain vs. Load Curve

Figure 51 displays the FEA solution for the strain at the loading condition of 540 N. Shown in Figure 51 are the top and bottom displays of the sample. The FEA solution shows an increase of strain around the hole compared to the locations away from the hole. This strain is less than the strain around the hole in Sample A; the patch is sharing the increased stress around the hole and therefore the region around the hole is exposed to less stress, which is related to strain via Hooke's law.

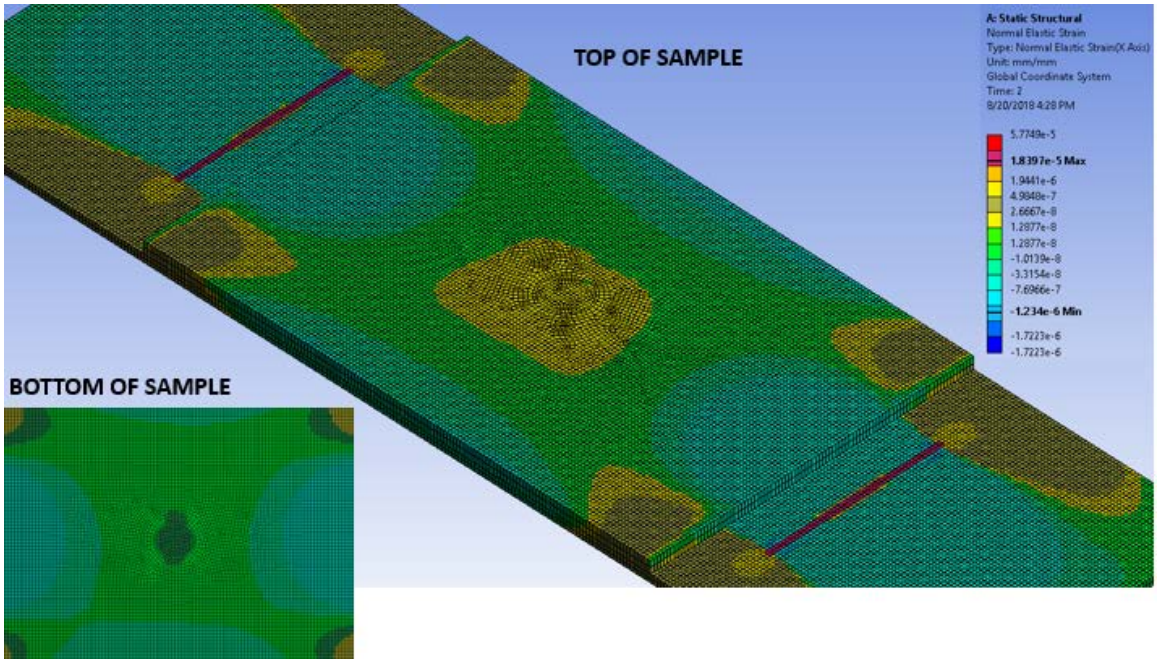

Figure 51. FEA Solution: Sample E at Loading Condition 540 N

Table 11. Sample E: Numerical vs. Experimental Strain at 540 N

	FEA	Experimental
Loading Condition [N]	540	540
Strain Value [με]	0.981	1.048

Analyzing the numerical data from the FEA at the location shown in Figure 49 and at the specified loading condition of 1017 N, the shear stress and normal stress in the y direction are

$$\tau_{XZ} = .10224\ MPa$$

$$\sigma_Y = 3.616E^{-4}\ MPa.$$

The Shear Stress, τ_{XZ}, is much larger of the two stresses indicating that if failure by delamination were to occur, it would have been due to shear stress. There was no delamination in Sample E, concluding that the interface strength for the patch is stronger than the interface strength of Sample C.

4. Samples G and H

The experimental results of Sample H are shown in Figure 52 displaying the strain (at hole) vs. load curve of the samples that have been repaired using the wet patching method described earlier and left in the water to cure for one week. Comparing the experimental results measured from the four point bending test and the numerical results derived from the FEA model at the specified loading condition of 540 N, there is a 16.23% difference in strain values, as shown in Table 12.

As shown in Figure 52, there is no point of delamination, nor does the sample reach a yield point. This specific test sample had a maximum loading condition of 937 N. Analyzing the strain vs. load curve of Sample A in Figure 46, Sample A has been loaded significantly past its yield point at 937 N.

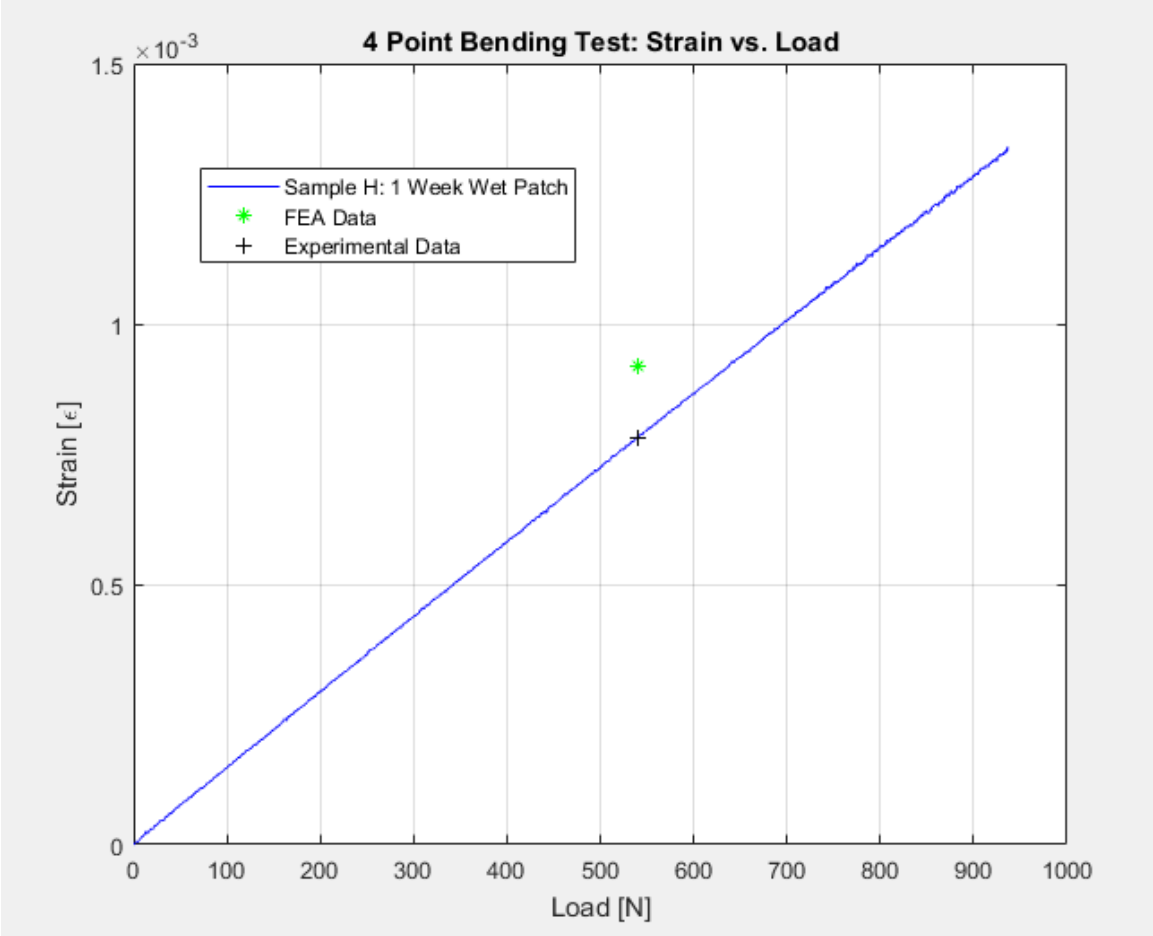

Figure 52. Experiment I: Sample H Strain vs. Load Curve

Table 12. Sample H: Numerical vs. Experimental Strain at 540 N

	FEA	Experimental
Loading Condition [N]	540	540
Strain Value [με]	0.919	0.7818

Analyzing the numerical data from the FEA at the location shown in Figure 49 and at the maximum loading condition of 937 N, the shear stress and normal stress in the y direction are

$$\tau_{XZ} = .1022\ MPa$$

$$\sigma_Y = 3.49E^{-4}\ MPa.$$

The shear stress is significantly larger than the normal stress in the y direction, indicating that if failure by delamination were to occur, it would have been due to shear stress. There was no delamination in Sample H, concluding that the interface strength for the patch is stronger than the interface strength of Sample C.

5. Samples I and J

The experimental results of Sample I are shown in Figure 53 displaying the strain (at hole) vs. load curve of the samples that have been repaired using the wet patching method described earlier and left in the water to cure for two weeks. Comparing the experimental results measured from the four point bending test and the numerical results derived from the FEA model at the specified loading condition of 540 N, there is a 12.74% difference in strain values, as shown in Table 13.

As shown in Figure 53, there is no point of delamination, nor does the sample reach a yield point. This specific test sample had a maximum loading condition of 1477 N. Analyzing the strain vs. load curve of Sample A in Figure 46, Sample A has been loaded significantly past its yield point at 1477 N.

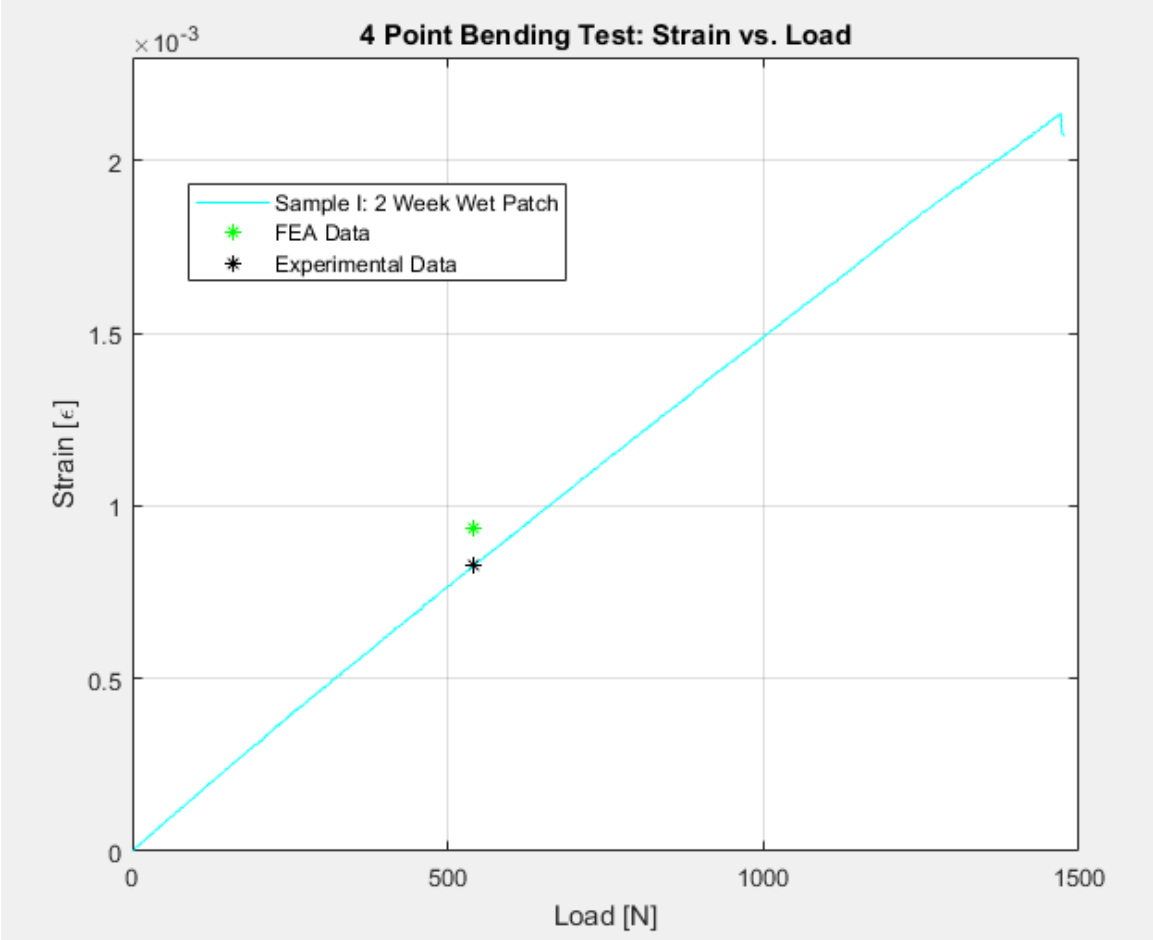

Figure 53. Experiment I: Sample I Strain vs. Load Curve

Table 13. Sample I: Numerical vs. Experimental Strain at 540 N

	FEA	Experimental
Loading Condition [N]	540	540
Strain Value [με]	0.823	0.935

Analyzing the numerical data from the FEA at the location shown in Figure 49 and at the maximum loading condition of 1477 N, the shear stress and normal stress in the y direction are

$$\tau_{XZ} = .0544\ MPa$$

$$\sigma_Y = 2.38E^{-4}\ MPa.$$

The shear stress is significantly larger than the normal stress in the y direction, indicating that if failure by delamination were to occur, it would have been due to shear stress. There was no delamination in Sample I, concluding that the interface strength for the patch is stronger than the interface strength of Sample C.

6. Samples K and L

The experimental results of Sample K are shown in Figure 54 displaying the strain (at hole) vs. load curve of the samples that have been repaired using the wet patching method described earlier and left in the water to cure for four weeks. Comparing the experimental results measured from the four point bending test and the numerical results derived from the FEA model at the specified loading condition of 540 N, there is a 10.52% difference in strain values, shown in Table 14.

The delamination point in which the patch began to physically separate from the aluminum in Experiment I Sample K occurred at loading condition of 1164 N and is depicted in Figure 54 as a red circle. Analyzing the numerical data from the FEA at the location shown in Figure 49 and at the specified loading condition of 1164 N, the shear stress and normal stress in the y direction are

$$\tau_{XZ} = .0409\ MPa$$

$$\sigma_Y = 1.39E^{-4}\ MPa.$$

The Shear Stress, τ_{XZ}, is much larger of the two stresses indicating the failure mode of delamination is due to shear stress for Sample K: 4 week wet patch.

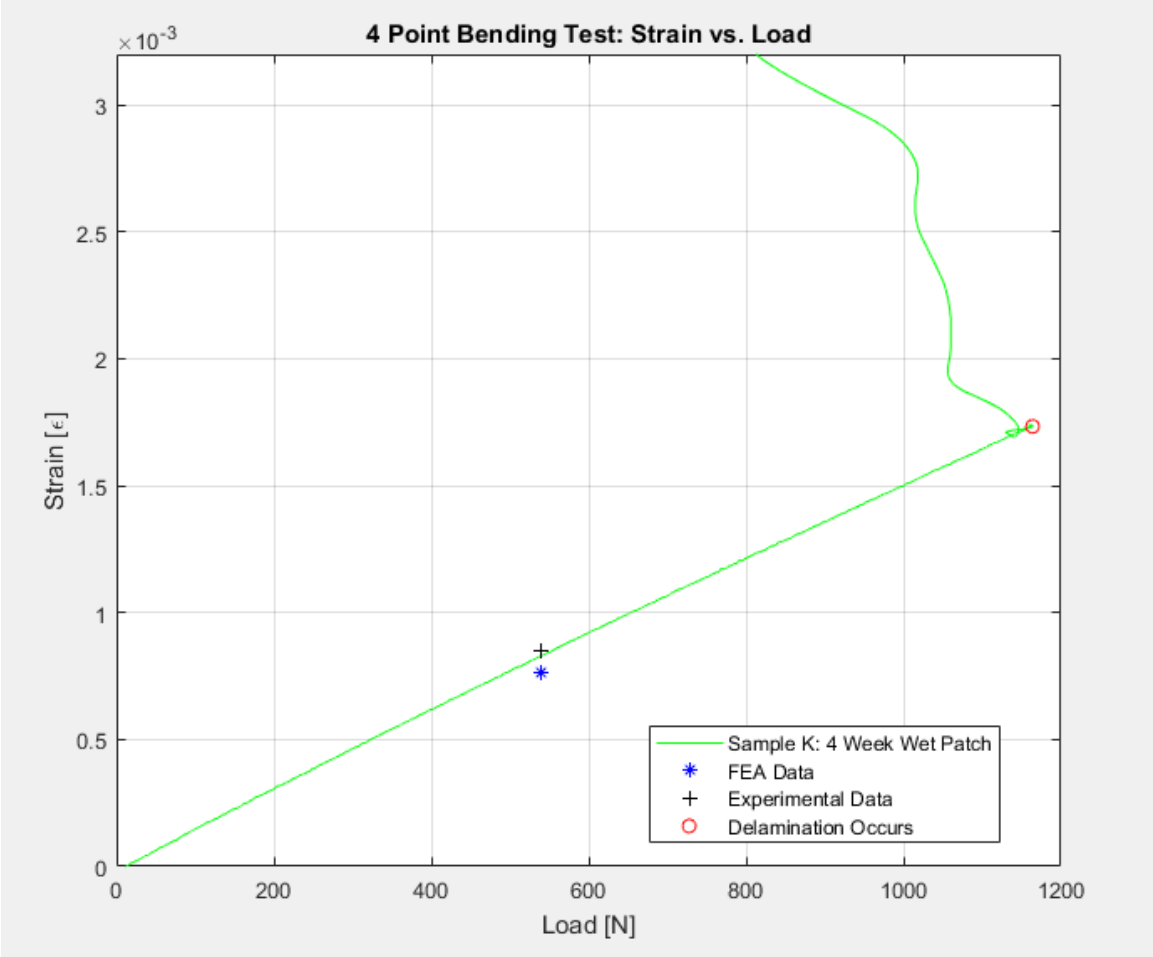

Figure 54. Experiment I: Sample K Strain vs. Load Curve

Table 14. Sample K: Numerical vs. Experimental Strain at 540 N

	FEA	Experimental
Loading Condition [N]	540	540
Strain Value [με]	0.8504	0.7654

7. Summary of Results: Experiment I

The first experiment, Experiment I, consisted of conducting a four-point bend test on twelve different samples, two samples for each of the six different categories. The

results of each testing category was presented and discussed in the previous section. By analyzing each sample and comparing them to each other, it is proven that the application of an underwater composite repair patch is effective in maintaining the structural integrity of the hull of an aluminum ship that has been degraded by an imperfection.

Looking at Figure 55 showing the strain vs. load curves for the first three categories of samples: no patch, dry patch, and 24 hour wet patch samples, it is shown that a composite repair patch applied to the damage underwater can significantly improve the material integrity. The strain experienced at the hole, which is directly related to stress, is significantly decreased when a repair patch is applied. The red solid line in Figure 55, is Sample A, with no repair patch applied. This aluminum sample reaches its yield point at 470 N and begins to enter the plastic region. Sample C, the sample with a dry repair patch, does not reach a yield point, but failure mode of delamination is reached at 1070 N. Sample E, the sample with a wet repair patch, does not reach a yield point and delamination of patch is shown.

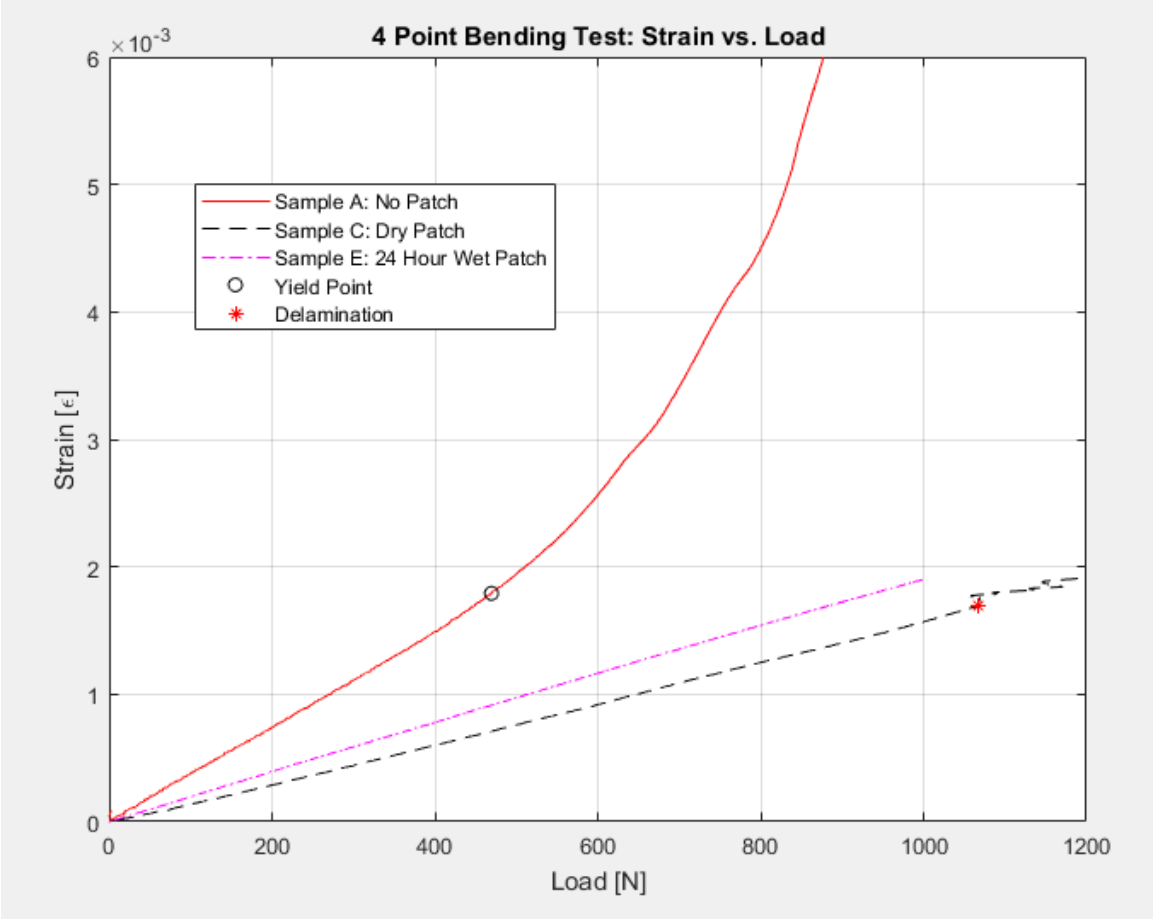

Figure 55. Experiment I: No Patch, Dry Patch, Wet Patch Samples Strain vs. Load

One of the concerns with the application of a composite repair patch is the patch failing by delamination. The interface strength, or bonding strength, is a function of both shear stress in the XZ direction and the Normal stress in the Y direction. Both stresses contribute to the delamination failure. However, if one stress is much larger than the other, the larger one will be the dominant stress causing the delamination. Both stresses were derived for all samples using the numerical data from the FEA models. In all cases, the shear stress was much larger out of the two. The shear stress at the maximum loading condition for all samples are shown in Table 15.

Table 15. Samples C-K: Shear Stress from FEA models

SAMPLE	Loading Condition [N]	Shear Stress [Mpa]
C: Dry Patch	1070	0.0102
E: 24 Hr Wet Patch	1017	0.10224
H: 1 Wk Wet Patch	937	0.1022
I: 2 Wks Wet Patch	1477	0.0544
K: 4 Wks Wet Patch	1164	0.0409

When compared to Sample C, Samples E and Samples H have a 164% higher shear stress, but proved in the experiment to not experience failure due to delamination like Sample C. Sample I has a 136.84% higher shear stress, and did not experience failure due to delamination. Sample K has a 120.17% higher shear stress, and experienced failure of delamination at 1164 N (9% higher loading condition) than Sample C. This has shown that the interface strength between the patch and the aluminum sample is significantly stronger when the patch is left in the water to cure.

All samples that were patched in the water are shown comparing the strains vs. loads in Figure 56. This graph shows that after at least one week of conducting the underwater repair patch procedure, the patch can effectively decrease the strain and stress in the material by at a minimum of 200%, when compared to 24 hours after the repair has been conducted.

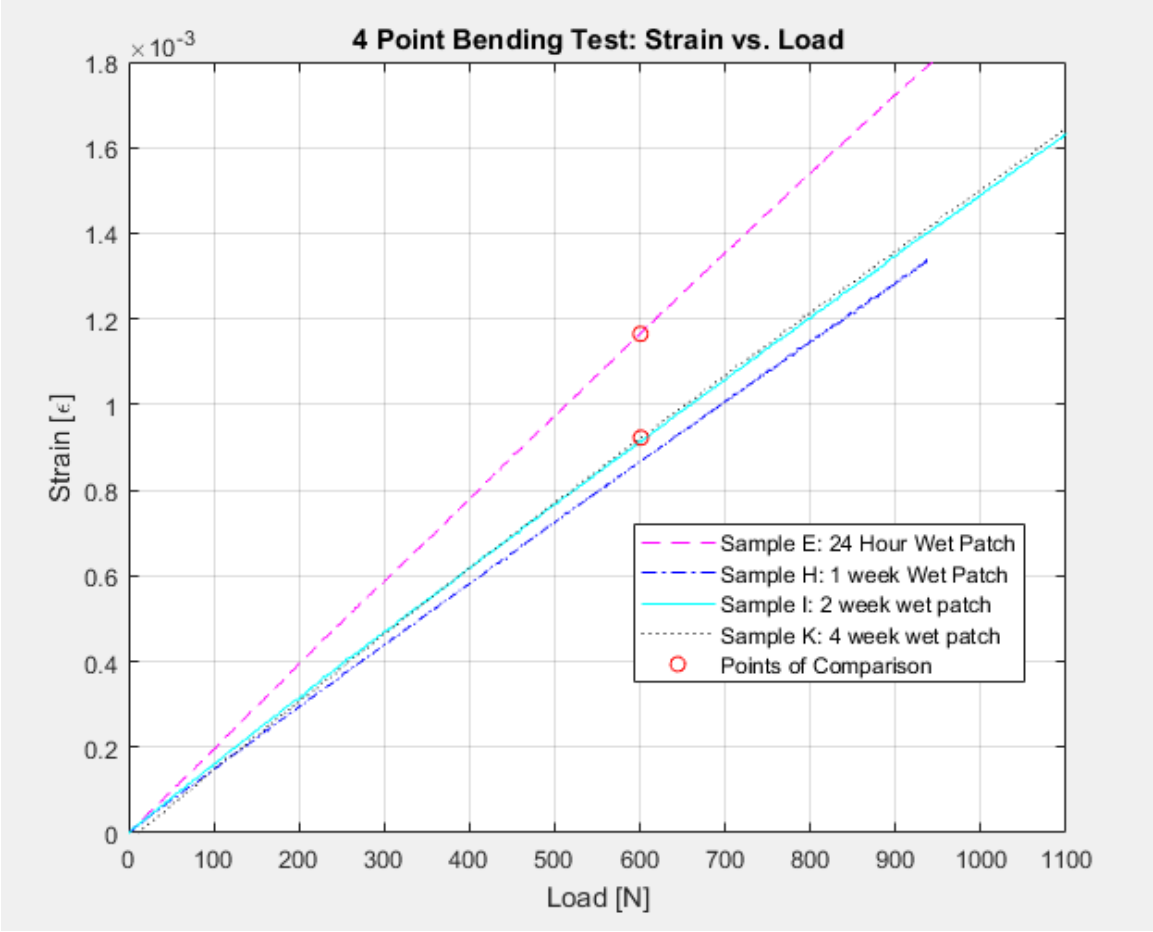

Figure 56. Experiment I: Wet Patched Samples Strain vs. Load

All samples of Experiment I are shown comparing the strains vs. loads in Figure 57. This graph proves that an underwater composite repair patch is extremely effective in decreasing the strain and by using Hooke's law, decreasing the stress in the material for a sample with a hole.

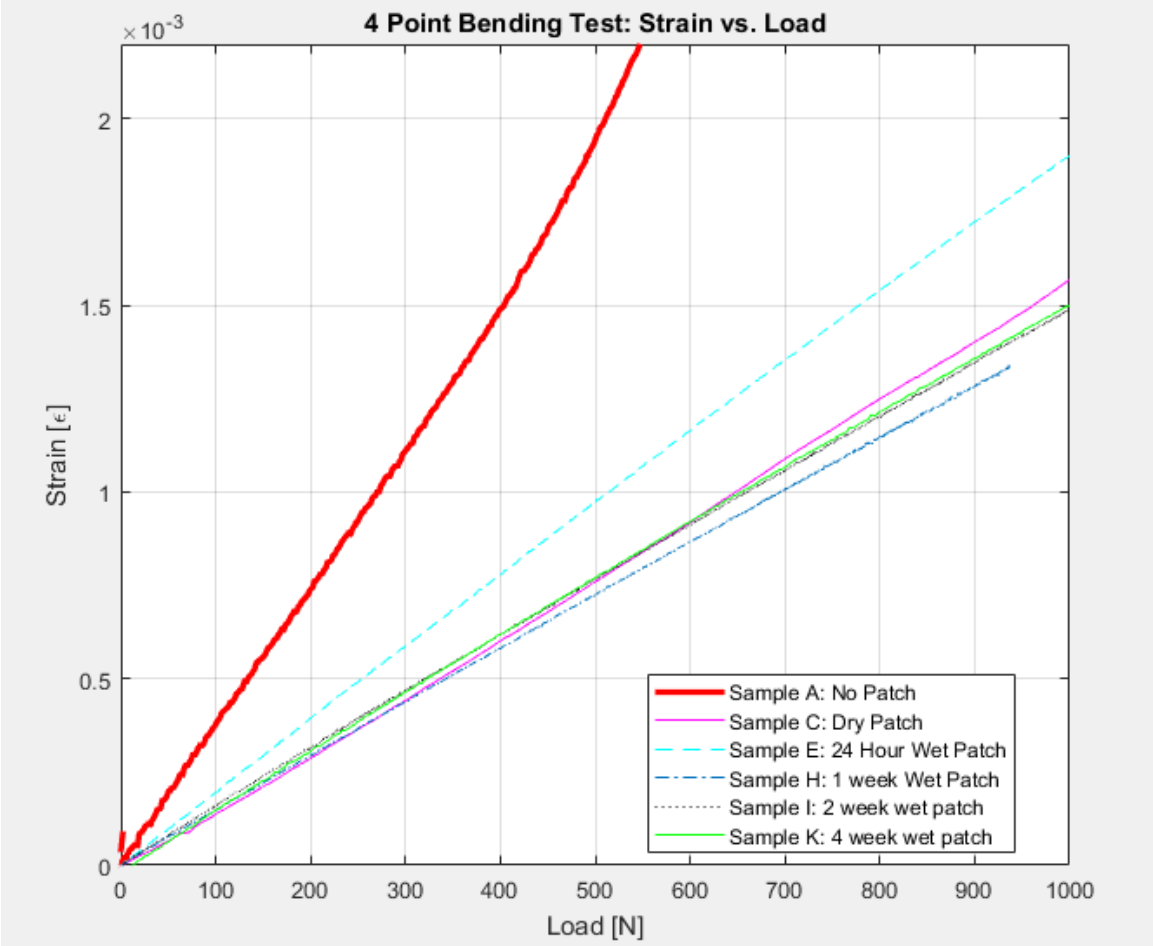

Figure 57. Experiment I: All Samples Strain vs. Loading

C. EXPERIMENT II: TENSILE TESTING

The Tensile testing analysis and calculations are treated as a composite beam formed from two materials, Aluminum and a Composite Patch. During Experiment II this composite beam is subjected to a purely axial force. The axial nominal stress Equation for the Aluminum Sample shown in Equation (10) was derived from modeling the sample as two separate beams in tension shown in Figure 58.

The following assumptions are made for further mathematical development.

The Aluminum sample and Composite patch have equal strains and are constrained to have equal displacements (prior to delamination of patch to sample). The areas of each sample are defined as width times the thickness. The width are assumed to be equal.

$$\varepsilon_1 = \varepsilon_2$$

$$u_1 = u_2$$

$$A_1 = w_1 t_1$$

$$A_2 = w_2 t_2$$

$$w_1 = w_2$$

Under uniaxial loading conditions, Hooke's law states:

$$\varepsilon_{xx} = \frac{\sigma_{xx}}{E} = \frac{F}{AE}$$

$$\frac{F_1}{A_1 E_1} = \frac{F_2}{A_2 E_2}$$

$$F_1 = \frac{F_2}{t_2 E_2}(t_1 E_1).$$

The total force carried in the sample combined is equal to the total force exerted by the INSTRON machine (P):

$$F_1 + F_2 = P$$

$$\frac{F_2}{t_2 E_2}(t_1 E_1) + F_2 = P$$

$$F_2\left(1 + \frac{t_1 E_1}{t_2 E_2}\right) = P.$$

The total force carried in the Aluminum Sample is defined as

$$F_2 = \frac{P}{1+\frac{t_1 E_1}{t_2 E_2}}.$$

The nominal axial stress carried in the Aluminum Sample is defined by Equation (10) and the strain that is experienced far away from the hole is calculated from Hooke's law shown in Equation (11) and can be compared to the measured strain gauges away from the hole.

$$\sigma_{2axial} = \frac{F}{A} = \frac{P}{A_2\left[1+\frac{t_1 E_1}{t_2 E_2}\right]} \quad (10)$$

$$\varepsilon_2 = \frac{\sigma_{2axial}}{E_2} = \frac{F}{A_2 E_2} = \frac{P}{A_2 E_2 [1+\frac{t_1 E_1}{t_2 E_2}]} \quad (11)$$

The concentration factor used to calculate the concentrated stress due to the hole in the Aluminum Sample was derived from the FEA model by strain measured at the hole and the strain measured away from the hole. Since strain and stress are related by Hooke's law, this concentration factor can be used in calculating the concentrated stress. K is defined in Equation (12). Equation (13) shows the Equation used in Experiment II's concentrated stress calculations.

$$K = \frac{\varepsilon_{Hole}}{\varepsilon_{Away\ from\ Hole}} \quad (12)$$

$$\sigma_{2axial} = K[\frac{F}{A}] = K[\frac{P}{A_2\left[1+\frac{t_1 E_1}{t_2 E_2}\right]}] \quad (13)$$

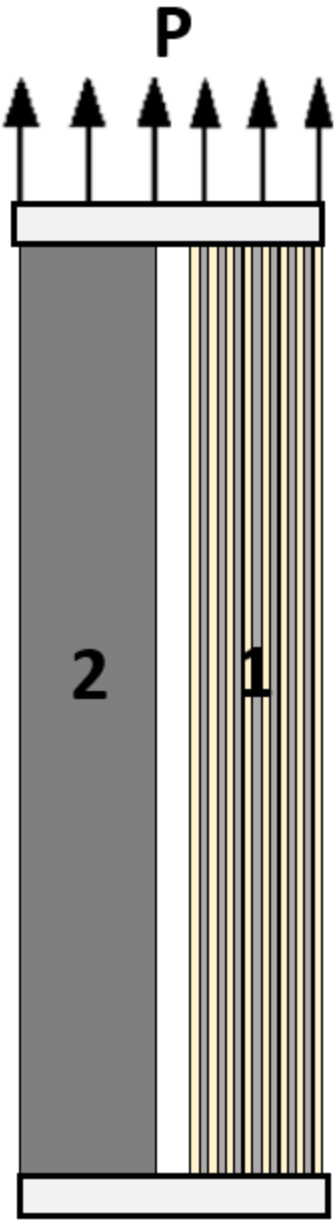

Figure 58. Tension Test Modeled as Two Separate Beams

The next experiment conducted was the tensile testing on all samples in the testing matrix shown in Table 2. This experiment was conducted to examine and analyze the effects of a purely axial load on the composite repair patch. Figure 59 compares the strain vs. load curves for Sample A, C, and E. As seen in Figure 59, the samples with a patch applied significantly decreases the strain over the loading conditions in the test. Also

displayed in Figure 59, is that the application of the patch increases the load condition in which the sample reaches its yield point without the patch. Sample A, the no patch sample, reaches its yield point at approximately 10,000 N, whereas Sample E, the 24 hour wet patch, reaches its yield point 16,900 N.

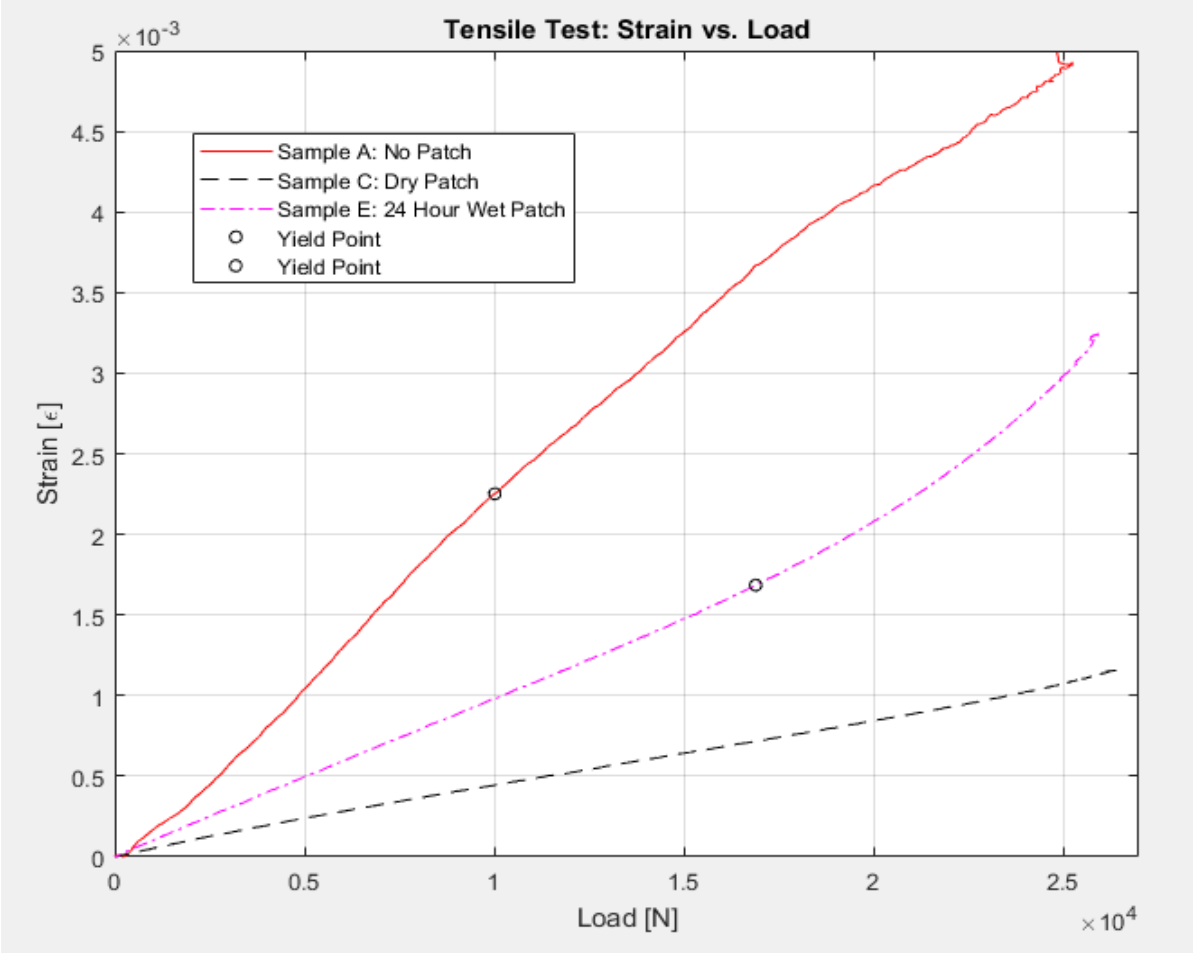

Figure 59. Experiment II: No Patch, Dry Patch, Wet Patch Strain vs. Load

The samples which were patched in the underwater environment and left in to cure for a variable amount of time are the Samples E-L. One sample from each time period is shown in a comparative graph of strain vs. load shown in Figure 60.

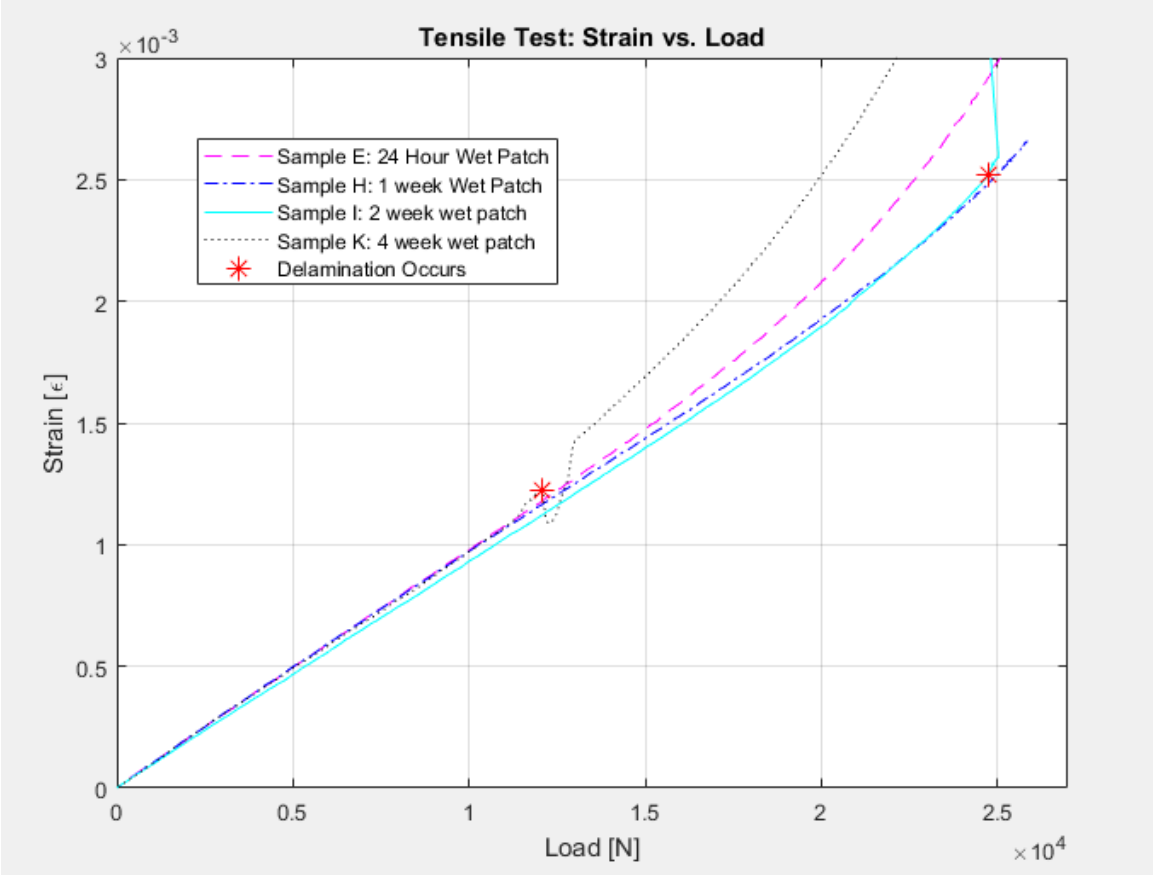

Figure 60. Experiment II: Wet Patched Samples Strain vs. Load

As seen in Figure 60, the samples that have been patched underwater and allowed to cure in the water for a different amounts of time perform very similar in the tensile test. There were two samples that experienced failure in the mode of delamination. These points are displayed by red stars in Figure 60. Analyzing the numerical data from the FEA of each patched sample tested in Experiment I, the shear and normal y stresses located at the patch interface was investigated. In Experiment II, the normal stress in the Y direction was significantly higher than the shear stress in the XZ direction. These two stress are the main contributors to a failure mode of delamination. Experiment II, tensile testing, the normal stress in the Y direction is the more dominant stress to consider for delamination causes. Table 16 displays this stress for each patched sample. For all samples that did not have delamination in the experiment, the normal Y stress is shown at the patch interface for the maximum loading condition. Samples I and K, the samples that failed due to delamination

in Experiment II, the normal Y stress is shown at the patch interface for the load in which the delamination occurred.

Table 16. Samples C-K: Normal Y Stress from FEA models

SAMPLE	Loading Condition [N]	Normal Y Stress[Mpa]
C: Dry Patch	26108.3	8.8749
E: 24 Hr Wet Patch	25726.98	9.7047
H: 1 Wk Wet Patch	25705.401	9.7106
I: 2 Wks Wet Patch	24740 *Delamination	9.0436
K: 4 Wks Wet Patch	12050 *Delamination	4.6941

Figure 61 and Figure 62 are the FEA models of Samples I and K. Shown are the top and bottom of the samples at the loads in which delamination occurred. The strains located at the holes of both of these models at the loading condition of delamination was compared to the experimental values. Table 17 show the values of the numerical model of the FEA and the experimental values. Percentage difference is also showed in Table 17. These values are displayed in the graph displayed in Figure 63. The FEA model is shown to accurately represent the strain in the aluminum sample with the repair patch applied. The numerical normal y stress values acquired from the FEA can be considered to be accurate.

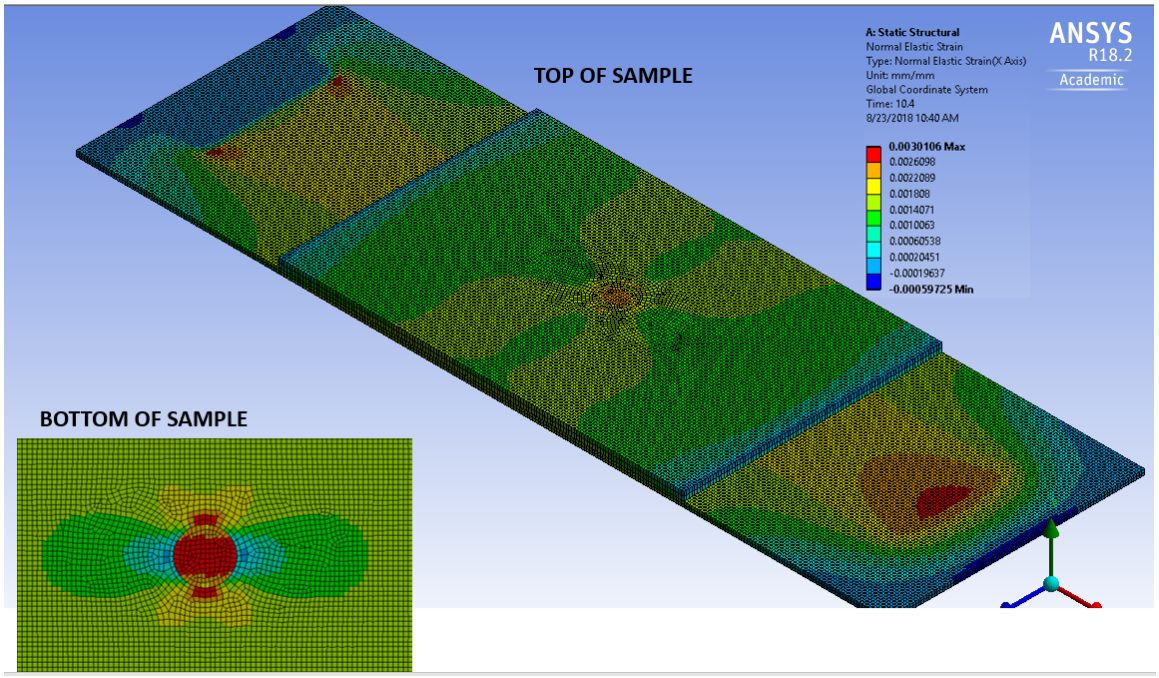

Figure 61. Experiment II: Sample I FEA at Delamination Loading Condition of $2.477E^4$ N

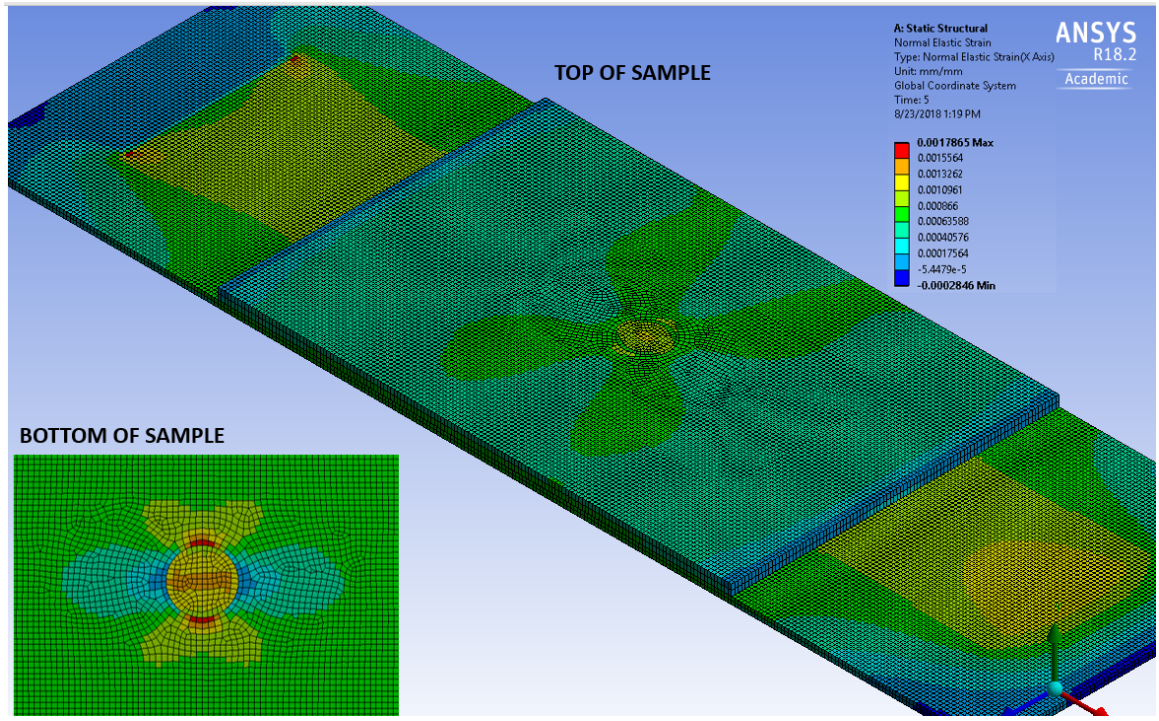

Figure 62. Experiment II: Sample K FEA at Delamination Loading Condition of $1.205E^4$ N

Table 17. Delaminated Samples I and K: Numerical vs. Experimental Strain Values

Sample I: 2 Wks Wet Patch	FEA	Experimental	Percent Difference
Loading Condition [N]	24700	24700	0
Strain Value [ε]	0.002409	0.00252	4.67%
Sample K: 4 Wks Wet Patch	**FEA**	**Experimental**	**Percent Difference**
Loading Condition [N]	12050	12050	0
Strain Value [ε]	0.001321	0.001224	7.54%

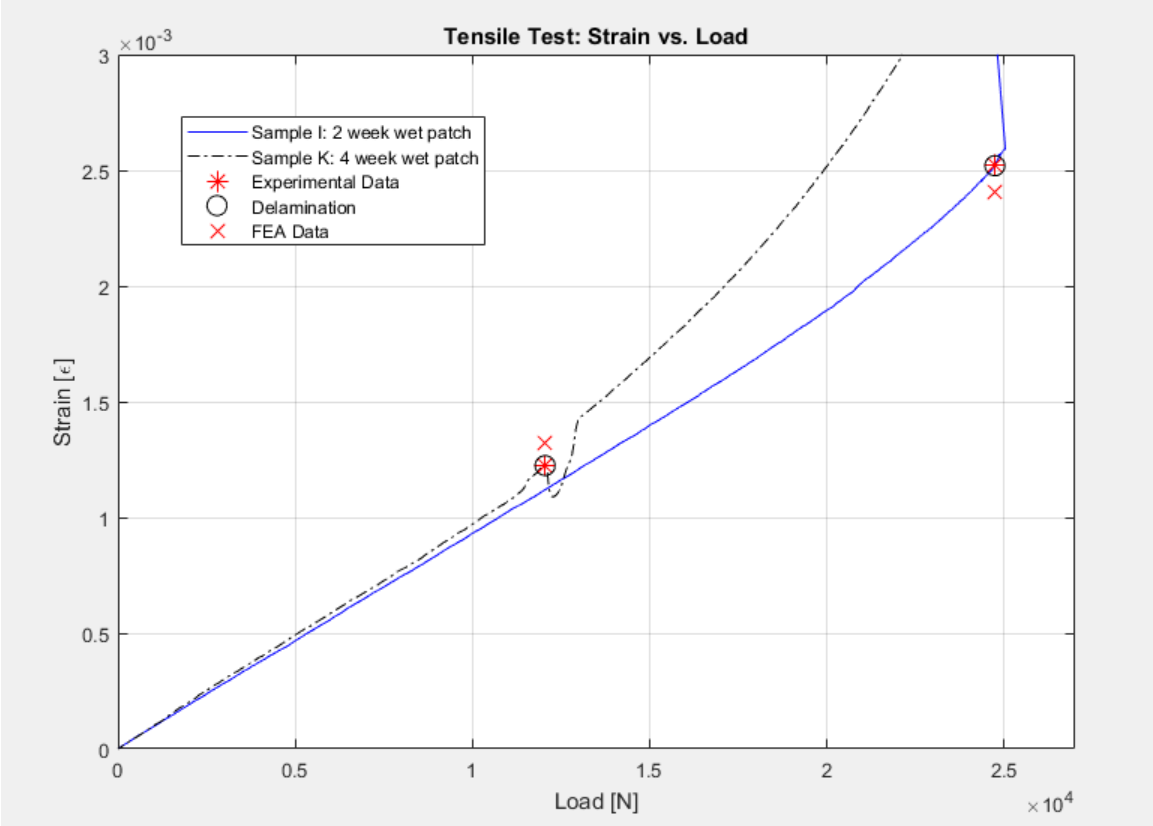

Figure 63. Experiment II: Delaminated Samples I and K Stress vs. Strain

D. OTHER EXPERIMENTAL OBSERVATIONS

During the testing phase of this thesis, the water absorption quality of this specific composite repair patch was investigated. An aluminum sample was patched using the dry repair patch procedure described earlier. This sample was immediately weighed and then placed in the underwater experimental tank. The sample was taken out of the water and

weighed at intervals of 24 hours, 1 week, 2 weeks, and 4 weeks. The results of the water absorption characteristics are summarized in Table 18. As shown, the composite repair patch had a 1.72% increase of mass after 168 hours (1 week) spent in the water. Additional exposure after 168 hours showed no further water absorption.

Table 18. Water Absorption of Composite Repair Patch

	Time spent in Water [hrs]	Mass [Kg]
Aluminum + Patch (Dry)	None	0.231
Aluminum + Patch (Wet)	24 hours	0.233
Aluminum + Patch (Wet)	168	0.235
Aluminum + Patch (Wet)	336	0.235
Aluminum + Patch (Wet)	672	0.235

Another important observation to note is the water solubility characteristics of the composite repair patch. While the experimenter was conducting the underwater repair patch procedure, during the application of the patch to the surface of the aluminum there was a small amount of epoxy released from the patch and into the water in the form of a sticky and thick film. This might have caused the original thickness of the design patch to be decreased and a variance in sample thicknesses across all experiments. It is recommended to build up the patches thicker in the topside preparation step in order to account for the loss experienced when taken underwater.

IV. DISCUSSION, CONCLUSION, AND RECOMMENDATIONS

A. DISCUSSION

Prior to the current research effort conducted for this thesis, there was no document that discussed the possibility or feasibility of conducting an underwater composite patch repair on aluminum hulls by U.S. Navy Divers. There have been no studies conducted that provides guidance on how to design, manufacture, and install an underwater composite repair patch onto the hulls of ships. This research and experimentation has been conducted based on the U.S. Navy's composite repair patch above water procedure and the experience of the researcher's exposure as a U.S. Navy Diving Officer. The results presented in this study involved repairs that were all conducted horizontally in a controlled lab tank and setting. In the real world environment, the application of such a composite repair patch would be conducted vertically on the side of the hull with growth and corrosion on the location of the repair. This must be considered during future research. The material selected for the composite repair patch, the techniques used in the fabrication of the composite repair patch, and the installation techniques used in the implementation of the repair patch onto the samples are subject to potential and expected improvements. Provided below is a list of possible improvements that should be considered for future research prior to the acceptance of this repair technique:

Selection of the composite material: E glass vs. Carbon

Selection of underwater epoxy

Selection of patch fabrication methods: wet-layup vs. pre-preg

Overall design of the patch: Selection of the fiber direction and thickness of patches

B. CONCLUSION

The overall goal of this study was to provide initial testing data to support the hypothesis that a composite repair patch can be effectively employed in the underwater

environment to an aluminum hull of a damaged ship. Two different experiments were conducted, Experiment I: Bending loading and Experiment II: Tensile loading. These were conducted to provide a baseline of data for comparison and analysis of a single sample with a defect that has been repaired by an underwater composite patch. These two experiments were conducted to test the durability and effectiveness of the patch in two separate loading conditions-bending loads and tensile loads. During the design of a repair patch, the minimum properties to determine for the composite material include stress, strain, and elastic modulus. In this study, the stress equations and the elastic modulus of each different composite patches was derived. The most important value assessed and used as a comparison for effectiveness of the patch was the strain in the aluminum measured at the defect. In both experiments, for all samples, the strain at the hole was measured and used to identify if the composite repair patch provided adequate reinforcement to reduce the strain in the aluminum samples.

The underwater repair patches did provide adequate reinforcement and the strain measured at the hole over the entire loading condition proved to be significantly lower than the sample without the patch. From a design failure standpoint, the numerical model of the FEA was used to assess the shear stress and normal stresses at the interface of the patch to identify what was the dominant stresses during delamination. It was shown in Experiment I, the shear stress was the dominant stress to investigate and in Experiment II, the normal y stress was the dominant stress to investigate. For both Experiments, it was proven that the interface strength between the patch and the aluminum surface was increased as the patch was allowed to cure in the water longer. The primary loading conditions a naval vessel would experience in normal operating conditions were tested and it was proven that individually tested, the patch is effective. This is an indication that in a combined loading condition, the patch would prove to be effective as well. The conclusion is that the underwater composite repair patch satisfied the research objective and that it is possible to repair ship hulls using a composite material.

C. RECOMMENDATIONS

For future research it is recommended to conduct further load testing to include combined loading conditions as well as cyclic loading conditions. It is also recommended to investigate whether this repair procedure could be considered for a longer-permanent repair, or be categorized as a temporary emergent repair. The long-term strength of the patch and the interface strength should be tested as well. Other recommendations include different testing environments such as varying the water temperature, salinity, marine growth.

If this underwater composite repair patch procedure is considered for future naval applications, the potential for inconsistency in fabrication and application should also be considered. It is recommended that a NAVSEA technician fabricate the repair patch above the water on site of the intended repair. The patch should then be immediately sealed so as not to expose the patch to humidity and water. Once sealed, the patch should be provided to the U.S. Navy Divers onsite to bring down to the depth of repair. Prior to the fabrication of the patch, the surface of the repair site should be thoroughly cleaned and fresh water should be used to ensure all marine growth is removed. Once the divers bring the sealed patch down to depth of repair, the patch should be opened and immediately placed on site of repair. The diver should apply pressure and ensure all air bubbles are squeegeed out of the patch. The patch should then be covered by a protective sleeve while the patch is being cured. After 24–28 hours of cure time, the patch should be painted with a protective sealant paint so as to ensure no water absorption occurs.

THIS PAGE INTENTIONALLY LEFT BLANK

APPENDIX A. PATCHING PROCESS PHOTOS (DRY AND WET)

Figure 64. Dry Patching Process Photos

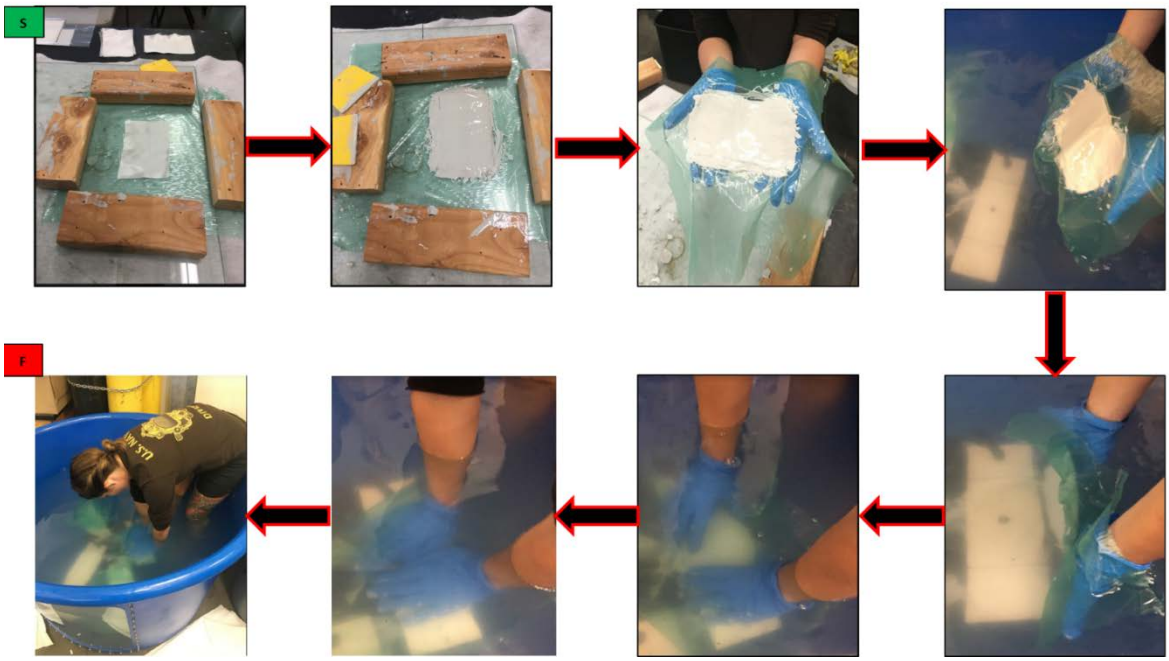

Figure 65. Wet Patching Process Photos

THIS PAGE INTENTIONALLY LEFT BLANK

APPENDIX B. EXPERIMENT I: STRAIN GAUGE PLACEMENT

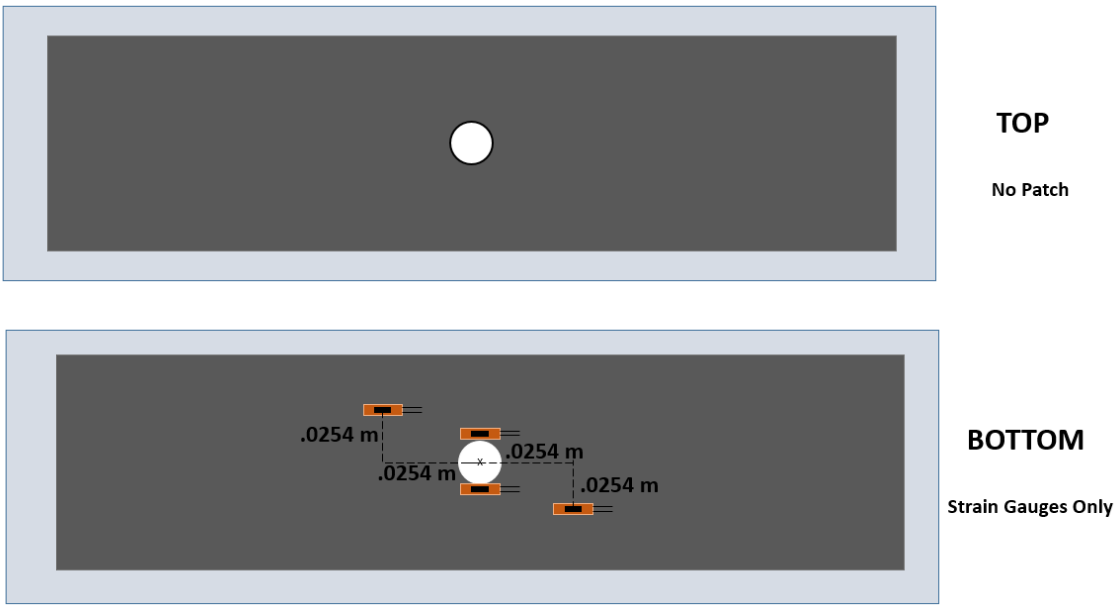

Figure 66. Experiment I: Sample A-B Strain Gauge Placement

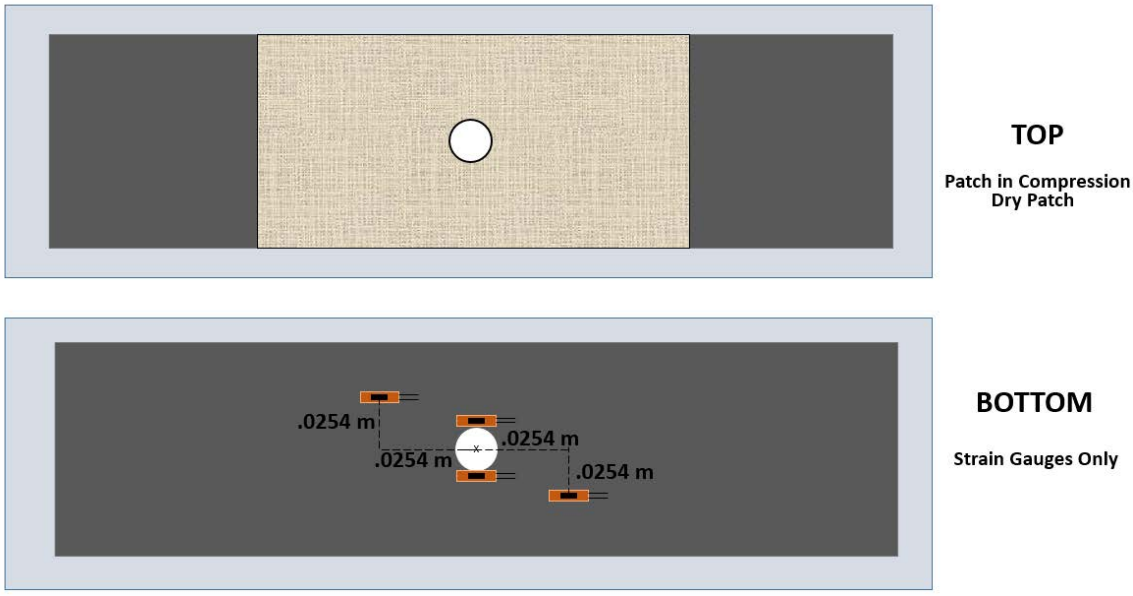

Figure 67. Experiment I: Sample C-D Strain Gauge Placement

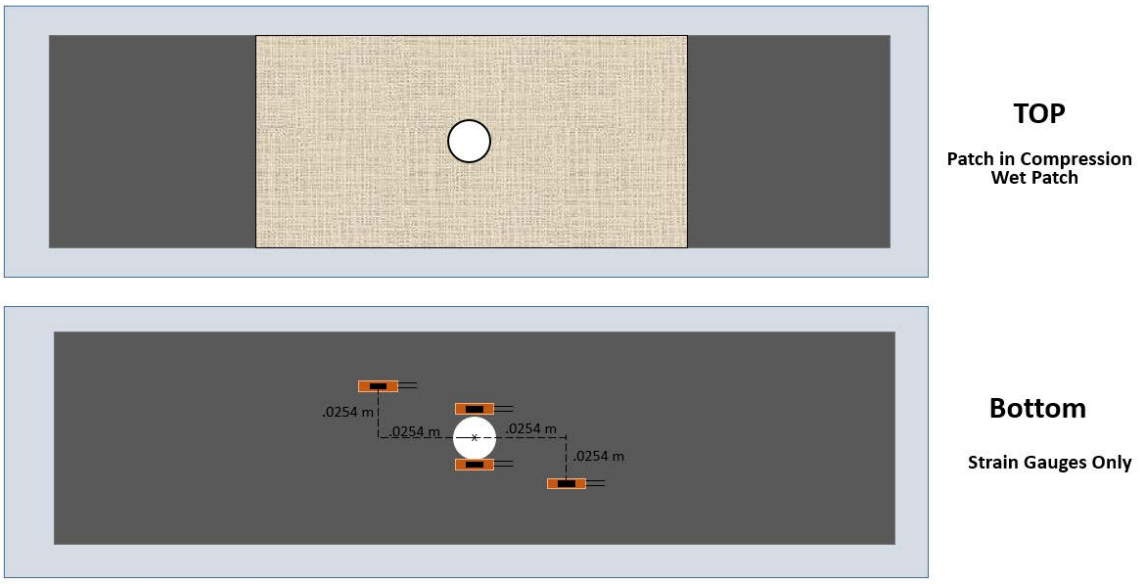

Figure 68. Experiment I: Sample E-L Strain Gauge Placement

APPENDIX C. EXPERIMENT II: STRAIN GAUGE PLACEMENT

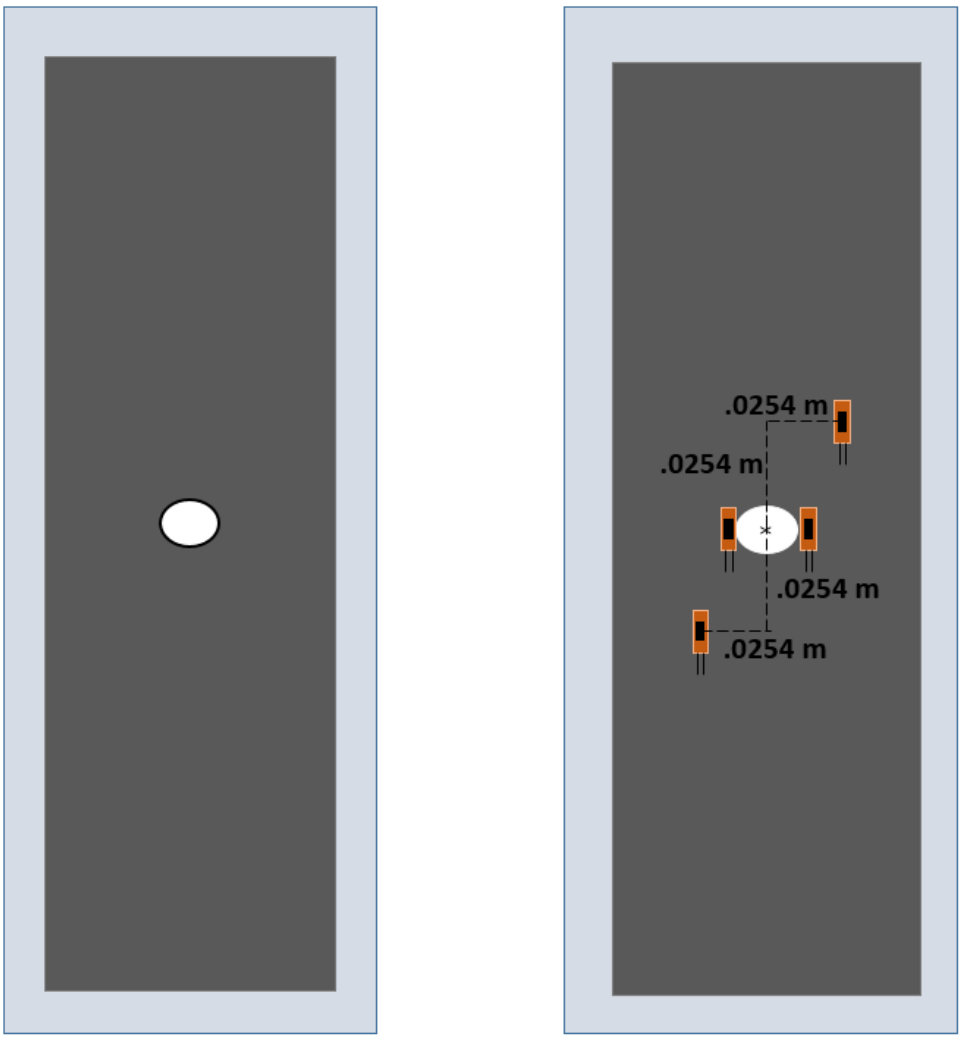

Figure 69. Experiment II: Samples A-B Strain Gauge Placement

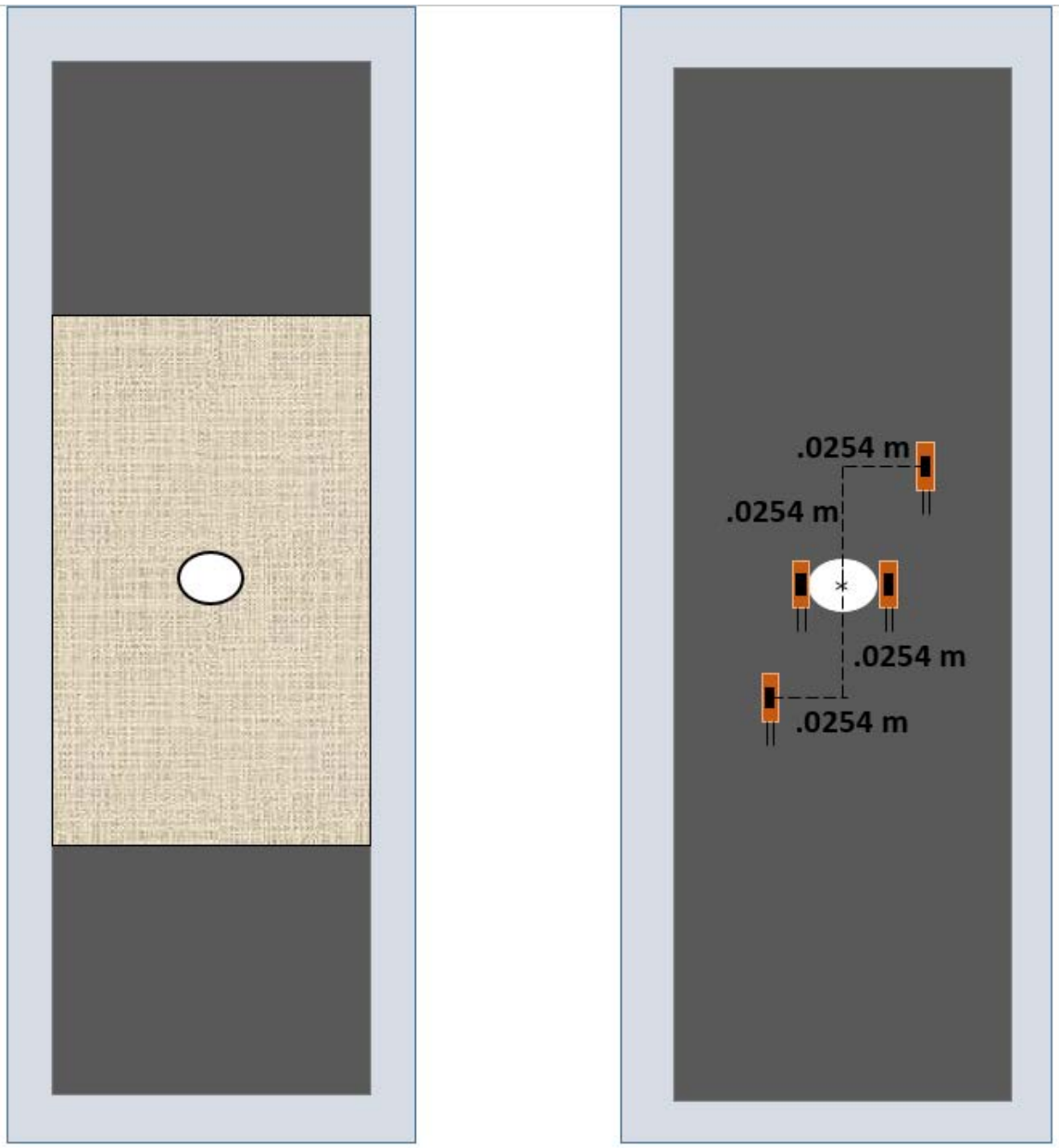

Figure 70. Experiment II: Samples C-L Strain Gauge Placement

LIST OF REFERENCES

[1] B. Needham and A. Field, "Sensitization of 5000 Series Al Alloys," Naval Surface Warefare Center Carderock Division, Corrosion and Engineering Branch, Mega Rust Report, San Diego, 2007.

[2] R. M. Jones, *Mechanics of Composite Materials*, 2nd ed., New York, NY: Taylor & Francis Group, LLC, 1999.

[3] ASTM, "ASTM G67-13;Standard Test Method for Determining the Suceptibility to intergranular Corrosion of 5XXX Series Aluminum Alloys by Mass Loss after Exposure to Nitric Acid (NAMLT Test)," ASTM International, West Conhohocken, PA, 2013.

[4] NSWC Program Office. email, May 2011.

[5] R. C. Allan , *Carbon Fibre Reinforcement of Weld Repairs to the Aluminium Alloy Superstructure of HMS Active,* Chicago: AMTE(S) TM83475, 1983.

[6] D. Hart and J. J. Noland, "Composite patch repair installation procedure for 5XXX aluminum alloy affected by stress corrosion cracking," Naval Surface Warfare Center Carderock Division, West Bethesda, MD, 2015.

[7] K. Suh, G. Mullins, D. Winters and R. Sen, "Use of FRP for Corrosion Mitigation Applications in a Marine Environment," Tampa Bay:ScienceDirect 2005.

[8] A. L. Corporation, *Aquawrap Repair System,* Pasadena,CA: Air Logisitics Corporation, 2003.

[9] F. C. LLC. “Material Data Sheet.” [Online]. Available: http://www.fyfeco.com/.

[10] D. Popineau and P. Wiet, "Subsea pipeline repair by composite system," in *Society of Petroleum Engineers*, Abu Dhai, 2012.

[11] Naval Sea Systems Command Technical Staff, *Naval Ship's Technical Manual Chapter 100,* Naval Sea Systems Command, 2010.

[12] *Tyfo SW-1 Epoxy Underwater Epoxy.* [Performance]. FYFE Co. LLC, 2015.

[13] U. Composites, "Fiberglass Cloth," U.S. Composites Inc, 2011. [Online]. Available: www.uscomposites.com/cloth.html. [Accessed 01 June 2018].

[14] ASTM, "ASTM G39-99:Standard Practice for Preparation and Use of Bent-Beam Stress-Corrosion Test Specimens," ASTM International, West Conhohocken, PA, 2016.

[15] E. Praire, *MTS Systems Corportation, Controller Installation and Calibration.* [Performance]. MN: MTS Systems Corporation, 1999.

[16] INSTRON, *5980 Series Dual Column Floor Frames,* Chicago, IL: Illinois Tool Works Inc. , 2009.

[17] R. Budynas, K. Nisbett and J. Shigley, *Shigley's Mechanical Engineering Design,* New York: McGraw-Hill, 2011.

[18] W. D. Pilkey, *Formulas for Stress, Strain, and Structural Matrices,* New York: Wiley, 1994.

[19] A. P. Boresi and R. J. Schmidt, *Advanced Mechanics of Materials,* New York: John Wiley & Sons, 2003.

[20] AZoM.com, "AZO materials," 30 August 2001. [Online]. Available: https://www.azom.com/article.aspx?ArticleID=764. [Accessed 09 08 2018].

[21] R. Schwarting, G. Ebel and T. Dorsch, "Manufacturing techniques and process challenges with CG47 class ship aluminum superstructures modernization and repairs," in *In Fleet Maintenace and Modernization Symposium 2001: Assessing Current and Future maintenace Strategies,* San Diego, 2011.

[22] K. K, "Offshore structural corner," 16 March 2017. [Online]. Available: kkurojjanawong.wordpress.com/2017/03/16/simplify-method-of-hogging-and-sagging-effect. [Accessed 20 June 2018].

INITIAL DISTRIBUTION LIST

1. Defense Technical Information Center
   Ft. Belvoir, Virginia

2. Dudley Knox Library
   Naval Postgraduate School
   Monterey, California